The Relationship between Q_γ and Ca Release from the Sarcoplasmic Reticulum in Skeletal Muscle

G. PIZARRO, L. CSERNOCH, I. URIBE, M. RODRÍGUEZ, and E. RÍOS

From the Department of Physiology, Rush University School of Medicine, Chicago, Illinois 60612

ABSTRACT Asymmetric membrane currents and fluxes of Ca^{2+} release were determined in skeletal muscle fibers voltage clamped in a Vaseline-gap chamber. The conditioning pulse protocol 1 for suppressing Ca^{2+} release and the "hump" component of charge movement current (I_γ), described in the first paper of this series, was applied at different test pulse voltages. The amplitude of the current suppressed during the ON transient reached a maximum at slightly suprathreshold test voltages (−50 to −40 mV) and decayed at higher voltages. The component of charge movement current suppressed by 20 μM tetracaine also went through a maximum at low pulse voltages. This anomalous voltage dependence is thus a property of I_γ, defined by either the conditioning protocol or the tetracaine effect. A negative (inward-going) phase was often observed in the asymmetric current during the ON of depolarizing pulses. This inward phase was shown to be an intramembranous charge movement based on (*a*) its presence in the records of total membrane current, (*b*) its voltage dependence, with a maximum at slightly suprathreshold voltages, (*c*) its association with a "hump" in the asymmetric current, (*d*) its inhibition by interventions that reduce the "hump," (*e*) equality of ON and OFF areas in the records of asymmetric current presenting this inward phase, and (*f*) its kinetic relationship with the time derivative of Ca release flux. The nonmonotonic voltage dependence of the amplitude of the hump and the possibility of an inward phase of intramembranous charge movement are used as the main criteria in the quantitative testing of a specific model. According to this model, released Ca^{2+} binds to negatively charged sites on the myoplasmic face of the voltage sensor and increases the local transmembrane potential, thus driving additional charge movement (the hump). This model successfully predicts the anomalous voltage dependence and all the kinetic properties of I_γ described in the previous papers. It also

Address reprint requests to Dr. Eduardo Ríos, Department of Physiology, Rush University School of Medicine, 1750 W. Harrison St., Chicago, IL 60612.

Dr. Pizarro's present address is Departamento de Biofísica, Facultad de Medicina, Montevideo, Uruguay. Dr. Csernoch's present address is Department of Physiology, University Medical School, Debrecen, Hungary, H-4012. Dr. Uribe's present address is Departamento de Fisiología y Biofísica, Facultad de Medicina, Universidad Autónoma de Chihuahua, A.P. 1090, Chihuahua, Chihuahua, México.

J. GEN. PHYSIOL. © The Rockefeller University Press · 0022-1295/91/05/0913/35 $2.00
Volume 97 May 1991 913–947

accounts for the inward phase in total asymmetric current and in the current suppressed by protocol 1. According to this model, I_γ accompanies activating transitions at the same set of voltage sensors as I_β. Therefore it should open additional release channels, which in turn should cause more I_γ, providing a positive feedback mechanism in the regulation of calcium release.

INTRODUCTION

In the preceding papers of this series a number of interventions expected to interfere with the process of Ca release from the sarcoplasmic reticulum (SR) were shown to selectively reduce (or increase, in the case of caffeine) a delayed component of intramembranous charge movement, which includes the "hump" and is similar to the current defined by subtraction after 20 μM tetracaine. These interventions provide alternative definitions of I_γ, some of which are much more convenient than (although not necessarily equivalent to) the usual definition based on the effect of greater concentrations of tetracaine (Huang, 1982; Hui, 1983*a*).

One practical method is protocol 1, in which I_γ is defined as the difference between the total membrane current moved by a depolarizing pulse and the current moved by the same pulse when it follows a conditioning pulse placed 150–400 ms earlier (Csernoch, Pizarro, Uribe, Rodríguez, and Ríos, 1991). This protocol can be applied many times during an experiment, which renders it convenient for detailed quantitative studies. Using this protocol we examine here the voltage dependence of I_γ, and find that it goes through a maximum at intermediate voltages. This is inconsistent with the view that I_γ is carried by an independent set of molecules undergoing voltage-driven conformational changes.

The difference in membrane current induced by protocol 1 has a positive phase, coincident with the hump in total asymmetric current, followed by a negative phase. We often observed a negative phase or undershoot in the total asymmetric current, especially clear in the presence of millimolar concentrations of intracellular EGTA. The properties of this phase can be understood best if it is an intramembranous charge movement. Since it is reduced or eliminated by the interventions that reduce the hump, it may be considered part of I_γ (meaning that it should be generated by the same mechanism). As suggested in the first paper of this series (Csernoch et al., 1991), both the hump and the negative phase may be caused by binding of Ca^{2+} coming out of the SR to negatively charged sites on or near the voltage sensors. A quantitative model is shown to simulate in detail all the properties described.

In this view, Q_γ arises at the same set of voltage sensors as Q_β, and should add to the excitation–contraction (E–C) coupling effects of Q_β. This constitutes a positive feedback mechanism: by activating more voltage sensors, the change in local potential will cause opening of more SR Ca release channels; the resulting local increase of Ca^{2+} in turn will lead to more charge movement and further channel opening. Evidence in support of such a feedback mechanism, some of which has been presented in abstract form (Pizarro, Rodríguez, Csernoch, and Ríos, 1990), is presently being prepared for publication.

METHODS

The experiments were conducted on cut segments of twitch fibers of *Rana pipiens* and *Rana sphenocephala* mounted in a double Vaseline-gap chamber as described previously (Csernoch et

al., 1991). The solutions used are listed in Table II of that paper. The present experiments were in most cases conducted on slack fibers with EGTA-containing internal solutions. The experiments were performed at temperatures between 12 and 16°C. The pH of the internal and external solutions was titrated to 7.00.

Kinetic Calculation of Calcium Concentration

In most experiments the internal solution contained 0.8 mM of the Ca-sensitive dye antipyrylazo III (ApIII) to monitor changes in $[Ca^{2+}]_i$ (Ca^{2+} transients), which was done following the methods described in the first paper, with the important difference that kinetics of the calcium:dye reaction were explicitly taken into account.

The determination of the change in $[Ca^{2+}]_i$ from the change in absorbance of a Ca^{2+}-binding dye involves two steps. First, the change in concentration of calcium:dye complex is derived from the change in absorbance. In a second step, $[Ca^{2+}]$ is derived from the concentration of Ca:dye complex assuming a given stoichiometry and kinetics of the reaction. Baylor, Quinta-Ferreira, and Hui (1985*a*) have shown that the kinetics of the Ca^{2+}:ApIII reaction in situ are best described with an OFF rate constant of 700 s^{-1}. Since in this paper we are concerned with detailed kinetic simulations of the time course of I_γ based on $[Ca^{2+}]_i(t)$, we abandoned the

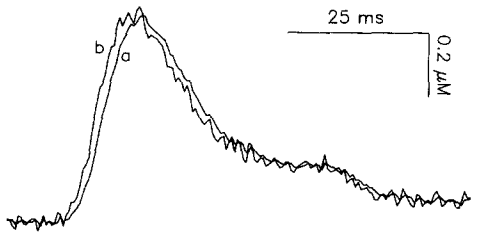

FIGURE 1. Ca^{2+} transients, equilibrium, and kinetic derivations. (*a*) Change in free Ca^{2+} concentration calculated from the absorbance change at 720 nm in the presence of 553 μM ApIII, assuming instantaneous equilibration and a dissociation constant of 30,200 μM^2. (*b*) Change in $[Ca^{2+}]$ derived with the kinetic Eq. 1 and the following values of rate constants: k_{on} = 0.023 μM^{-2} s^{-1}, k_{off} = 700 s^{-1}. Pulse to −50 mV (shown in Fig. 2). Holding potential, −90 mV. Fiber 612, at slack length, described in detail in legends to Figs. 2 and 3. External solution, reference. Internal solution, 8 EGTA. Temperature, 13°C.

assumption of instantaneous equilibrium used in our previous work (Kovacs, Ríos, and Schneider, 1983) and computed $[Ca^{2+}]$ with the equation

$$[Ca^{2+}] = ([CaD_2]k_{off} + d[CaD_2]/dt)/([D]^2k_{on}) \quad (1)$$

where D represents the dye, $[CaD_2]$ is the concentration of the calcium:dye complex derived from the absorbance change, and k_{on} and k_{off} are the rate constants. k_{off} is set to 700^{-1} and k_{on} = k_{off}/K_d, where K_d is the dissociation constant, calculated as described by Kovacs et al. (1983).[1]

Fig. 1 compares a Ca^{2+} transient calculated assuming instantaneous equilibration with one calculated kinetically. The one calculated kinetically is ~1.4 ms faster. It is also more noisy, due to the inclusion of a term proportional to the derivative of the optical signal (Eq. 1).

From the Ca^{2+} transients we obtained release flux by the method described in the first paper of this series (and in greater detail by Brum, Ríos, and Stefani, 1988*b*). This method requires the fitting of the decay of the Ca^{2+} transients after the pulse with a model of Ca^{2+} removal that

[1] Our device measures the change $\Delta[CaD_2]$ from a resting level. Eq. 1 uses the approximation $\Delta[CaD_2] \simeq [CaD_2]$, which is justified as the saturation of the dye is <0.1% at the nominal $[Ca^{2+}]_i$ in the internal solution.

includes intrinsic and foreign Ca^{2+}-binding molecules. In this description of removal of Ca^{2+} we included EGTA as an additional high affinity buffer, which becomes the predominant removal agent at the concentrations used in these experiments. We found that the decay of $[Ca^{2+}]_i$ in the presence of high [EGTA] can only be fitted assuming slow rates of binding, of the order of 10^{-6} M^{-1} s^{-1}, in agreement with the measurements of Smith, Liesegang, Berger, Czerlinski and Podolsky, (1984). A comparative study of Ca release in the presence of EGTA and other extrinsic buffers is in progress (Ríos, Brum, Pizarro, and Rodríguez, 1990).

Digital Filtering

The computation of release flux involves differentiation of the Ca^{2+} transients and that increases the noise in the derived waveform. For this reason the Ca^{2+} transients obtained kinetically were first digitally filtered. The filter used is defined by

$$y_i = (x_{i-2} + 4x_{i-1} + 6x_i + 4x_{i+1} + x_{i+2})/16$$

where x_i is the signal at interval i before filtering and y_i is the filtered value. This filter is a symmetric operation around interval i; therefore, it does not cause time shifts (although it will slightly change the time to peak of very asymmetric signals). It results from applying twice the simple three-point smoothing operation

$$y_i = (x_{i-1} + 2x_i + x_{i+1})/4$$

An example of its effect is given in Fig. 3.

Nomenclature of Currents

$\Delta I_a(t)$ represents the asymmetric current, defined as in Csernoch et al. (1991) as

$$\Delta I_a(t) = \Delta I_{test}(t) - [\Delta V_{test}/\Delta V_{control}]\Delta I_{control}(t)$$

where ΔI is total membrane current (measured from its initial level) and ΔV_{test} and $\Delta V_{control}$ are the changes in measured voltage V upon application of a test and a control pulse, respectively. Controls were 20-mV pulses from −130 mV unless otherwise indicated. None of the asymmetric currents presented here were corrected for ionic components. Two interventions were used to separate a component of current. $\Delta I_1(t)$ represents the current separated by protocol 1 (Csernoch et al., 1991) and is the difference between total currents ΔI elicited by a reference test pulse and a conditioned pulse of the same amplitude. $\Delta I_t(t)$ represents the current suppressed by 20 μM tetracaine (Csernoch et al., 1991). Based on arguments in the first paper, I_γ is used in this paper as equivalent to $\Delta I_1(t)$.

RESULTS

The first set of results regards the voltage dependence of $\Delta I_1(t)$, the current suppressed by protocol 1. The second set is a demonstration that similar properties are found in the current suppressed by 20 μM tetracaine. The third is a demonstration of a novel property in total intramembranous charge movement current, the existence of an inward phase during a depolarizing pulse.

Voltage Dependence of $\Delta I_1(t)$

Fig. 2 shows a family of asymmetric currents, constructed as differences between total membrane current during a test pulse (records of measured voltage at bottom) and a control pulse. Every pair includes a reference record and a conditioned record,

obtained with the test pulse preceded by a conditioning pulse. Reference and conditioned records were shifted vertically to superimpose the ends of the ON transients. The conditioning pulse, to 0 mV, had a 100-ms duration and ended 450 ms before the beginning of the test pulse. The fiber was at slack length (immobilized by 8 mM EGTA in the internal solution) in reference external solution.

As described in the first paper of this series, the conditioning pulse alters the asymmetric current, reducing the hump visible at intermediate voltages and prolonging the asymmetric current transient. It is clear in the figure that the conditioning pulse has very little effect at low voltages (the currents during the prepulse to −70 mV are practically unchanged). It appears that the effect at high voltages is also small.

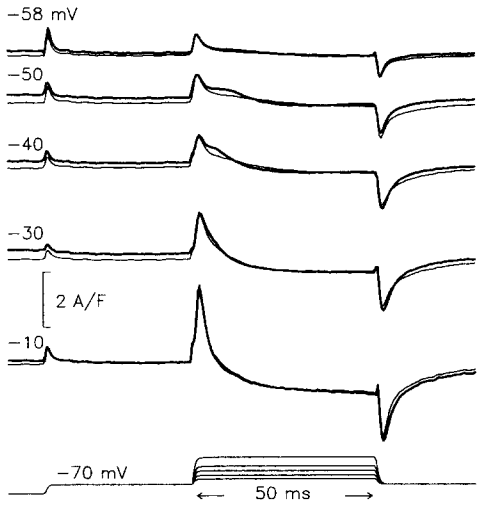

FIGURE 2. Protocol 1 at different voltages. (*Top*) Asymmetric currents obtained as differences between the total current (ΔI_{test}) during a test pulse and a control current. The recorded voltage $V(t)$ is shown at bottom. It is the result of scaling by 1.05 the voltage $V_1(t)$ in the voltage pool of the chamber. The control current is the sum of two currents, one for the prepulse to −70 mV and another for the test pulse. They are obtained with 30-mV pulses from −130 mV, of 245 and 100 ms duration, respectively, for pre- and test pulses, and scaled by the corresponding ratios of measured voltages. In every pair of asymmetric currents shown, the thick trace is reference and the other is conditioned by a pulse to −10 mV, of 100 ms, that ends 400 ms before the prepulse. Every reference test is a single sweep and every conditioned test is an average of four sweeps repeated at 5-s intervals. The control currents are the same (except for scaling) in all records. Capacitance in controls, 25.2 nF. Fiber 612. Holding potential, −90 mV. External solution, reference. Internal solution, 8 EGTA. Diameter, 128 μm. Sarcomere length, 2.6 μm. Temperature, 13°C.

Fig. 3 plots the Ca^{2+} transients derived from simultaneous optical measurements in the same experiment. The Ca^{2+} transients are small in amplitude and have the characteristic early peak of a release flux record (Melzer, Ríos, and Scheider, 1984). These characteristics are a consequence of the high EGTA in the internal solution. Each pair of records includes a reference and a conditioned transient. The conditioned transient is always smaller, lacking the characteristic peak. These records of $[Ca^{2+}]_i(t)$ will be used later in detailed simulations of I_γ. Since they are noisy (because they are small and because of the kinetic technique for derivation of transients; cf. Methods) they were digitally filtered before further analyses (as described in Methods). The filtered records at −10 mV are shown superimposed on the unprocessed records.

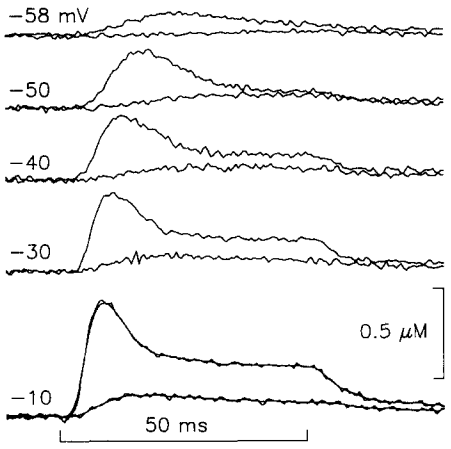

FIGURE 3. Ca^{2+} transients with protocol 1. Ca^{2+} transients derived with kinetic Eq. 1 from absorbance changes recorded simultaneously with the currents of Fig. 2. Optical methods for measuring absorbance changes and correcting for intrinsic components described by Csernoch et al. (1991). The conditioned transient is the smaller and slower record in each pair. All records were digitally filtered as described in Methods. Filtered records are shown superimposed on the original records at −10 mV.

Fig. 4 plots differences between the currents in Fig. 2 (reference minus conditioned). Since the same control record was used for all traces in Fig. 2, the differences between asymmetric currents are identical to the differences between total membrane currents (these differences induced by protocol 1 are termed $\Delta I_1(t)$). The difference in the current during the prepulse to −70 mV is steady. The current difference during the test pulse has the kinetic characteristics described in the previous papers and a steep voltage dependence, increasing rapidly from −58 to −50, and decreasing in amplitude beyond −40 mV as it becomes faster. This voltage dependence was observed consistently, in both slack and stretched fibers. It was less clear in stretched fibers, however, given the smaller size of $\Delta I_1(t)$ (Csernoch et al., 1991) and the fact that protocol 1 often suppressed an additional fast component of current in stretched fibers (for instance, Fig. 4 in Csernoch et al., 1991). Results of three experiments in slack fibers are summarized in Fig. 6.

Fig. 5 illustrates one of five experiments exploring the voltage dependence of the current suppressed by 20 μM tetracaine, $\Delta I_t(t)$, which in the previous papers was shown to have properties similar to $\Delta I_1(t)$. In these experiments test pulses to two

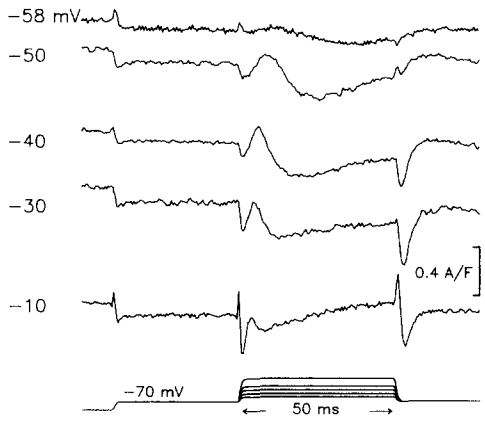

FIGURE 4. Current differences with protocol 1. (*Top*) Differences between reference and conditioned records in Fig. 2. Since the records in Fig. 2 are asymmetric currents constructed with the same control current, the records in this figure are identical to differences between total membrane current during reference conditioned pulses.

voltages were applied: a voltage at which the hump in the asymmetric current was clearly visible (−45 mV in the case illustrated) and a high voltage (0 mV). Then the external solution was replaced with one containing tetracaine and the pulses were repeated in reverse order. Control currents were obtained in both solutions. Usually the effects of tetracaine were rapidly reversible upon washout. The records on the left are asymmetric currents in both conditions. Tetracaine reduces the hump at −45 mV. Remarkably, the reference record at −45 mV also has an inward-going phase

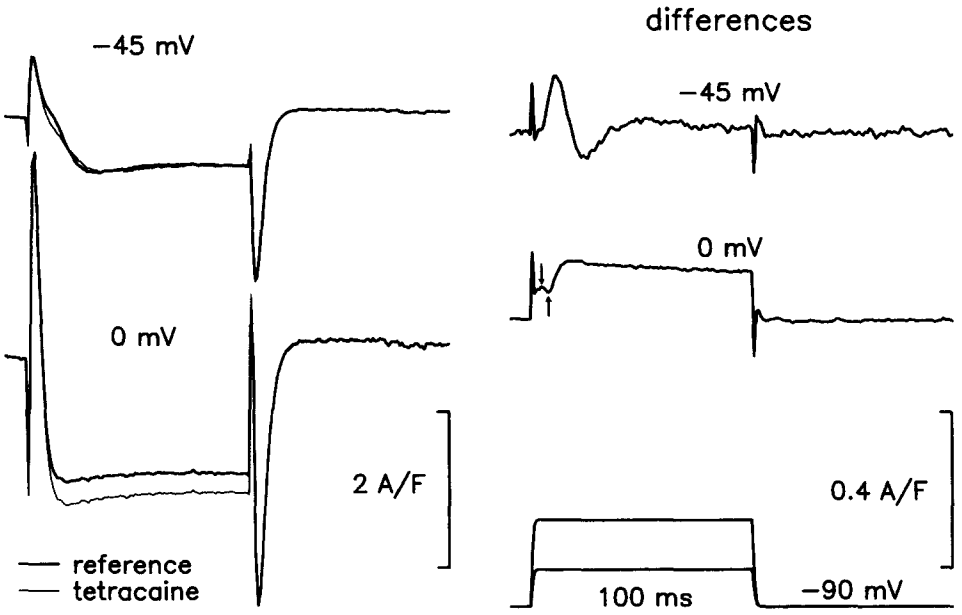

FIGURE 5. Effect of tetracaine at two voltages. (*Left*) Asymmetric currents during a pulse to the voltages indicated. Records in thick and thin traces obtained before and after exposure to 20 μM tetracaine, respectively. The control current is an average of currents before and after tetracaine. (*Right*) Differences between records at left (identical to differences of total membrane currents). In the record at 0 mV the arrows mark values used as minuend and subtrahend in the definition of amplitude of the current sensitive to tetracaine. Bottom records, $V(t)$. Fiber 549. External solution, Co-Ca. Internal solution, 15 EGTA (no ApIII). Linear capacitance, 19.4 nC/μF in reference and 19.8 nC/μF in tetracaine. Diameter and sarcomere length not measured. Temperature, measured at 12.4 and 13.8°C immediately before and after the solution change.

after the hump. This phase was clear in four of the five fibers, and was always slowed and reduced in amplitude by tetracaine. At 0 mV the effects are less obvious.

The differences between total currents are plotted on the right. The difference at −45 mV is very similar to the $\Delta I_1(t)$ records at −50 or −40 mV in Fig. 4. In the record at 0 mV it is possible to identify a small local maximum followed by a minimum (arrows), not unlike the extremes in the record at −10 mV in Fig. 4. A similar small peak is found in a comparable record in the first paper of this series

(Fig. 17 *B*, record at 0 mV; Csernoch et al., 1991). Similar peaks were found at 0 mV in three experiments. In two other experiments with tetracaine the peak was either absent or was too fast to be resolved.

Fig. 6 summarizes the study of voltage dependence of $\Delta I_1(t)$ in slack fibers and the results from the three experiments with tetracaine in which the outward-going phase could be resolved at the higher voltage. Plotted are the amplitudes (maximum minus minimum) of $\Delta I_1(t)$ (open symbols) and $\Delta I_t(t)$ (filled symbols). The amplitude of $\Delta I_1(t)$ goes through a maximum at intermediate voltages. This maximum is similar to the amplitude of the tetracaine-sensitive current in this voltage range. This transient outward component is very small in the tetracaine differences at 0 mV.

A Negative Phase in Total Charge Movement Current

A negative-going phase in the asymmetric current can be seen during the ON in the records at −45 mV in Fig. 5, in the records of Figs. 1, 13, 17, and 18 in Csernoch et

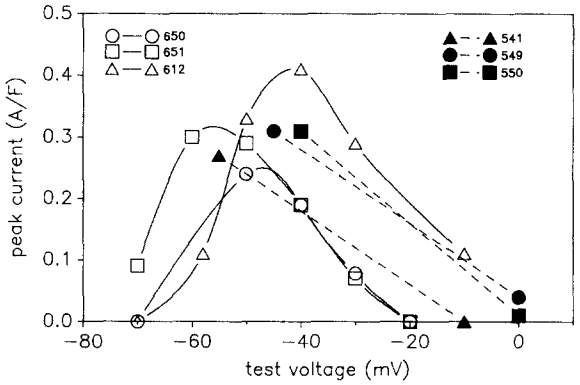

FIGURE 6. Voltage dependence of I_γ by protocol 1. *Open symbols*, amplitude of current suppressed by protocol 1. *Filled symbols*, amplitude of current suppressed by 20 μM tetracaine. Amplitudes were measured from transient peak to transient minimum during the ON. Different symbols correspond to different fibers. All fibers were at slack length in internal solutions 8 EGTA (all protocol 1 experiments) or 15 EGTA (tetracaine experiments). The external solution was reference (612), 10 Ca (650, 651), and Co-Ca (tetracaine). Linear capacitances in controls (in nC/μF, listed in the order of increasing fiber numbers): 7.45, 19.6, 22.2, 25.2, 32.0, and 18.1. Temperatures, 12–14°C.

al. (1991), in Figs. 1 and 4 of García, Pizarro, Ríos, and Stefani (1991), and in Figs. 1, 4, and 6 in Szűcs, Csernoch, Magyar, and Kovács (1991). Similar phases can be found in earlier work. Normally they are dismissed as an indication of small time-dependent ionic currents in test and/or controls and excluded from the calculation of areas through baseline subtraction. However, in work with slack fibers with intracellular EGTA they become too large to be ignored. They appear consistently in asymmetric currents with a visible hump and they share with the hump the close correlation with E-C coupling. We believe that in these cases they correspond to actual inward-going intramembranous charge movement.

Fig. 7 illustrates one of many cases in which this component was large. *B* plots the asymmetric currents at the voltages indicated. These records illustrate two aspects of the inward-going phase: it appears at approximately the same voltage as the hump, and it becomes smaller at high voltages (as seen for the amplitude of I_γ in the previous sections). The total membrane currents are plotted in *A* and illustrate

another important aspect: the inward-going phase is not the result of subtraction of control currents. The total membrane currents represented in *A* have an inward-going phase, riding on a pedestal of outward current, at −37 and −32 mV. This phase is not visible in the other records, at higher or lower voltages.

A similar inward phase in total membrane current was present in seven other experiments on slack fibers with EGTA, all of which had prominent humps in the asymmetric current. Negative phases in total current were never observed in stretched fibers, but small negative phases in asymmetric currents were found in three of the seven fibers listed in Table III of Csernoch et al. (1991). One example is illustrated in Fig. 1 of that paper.

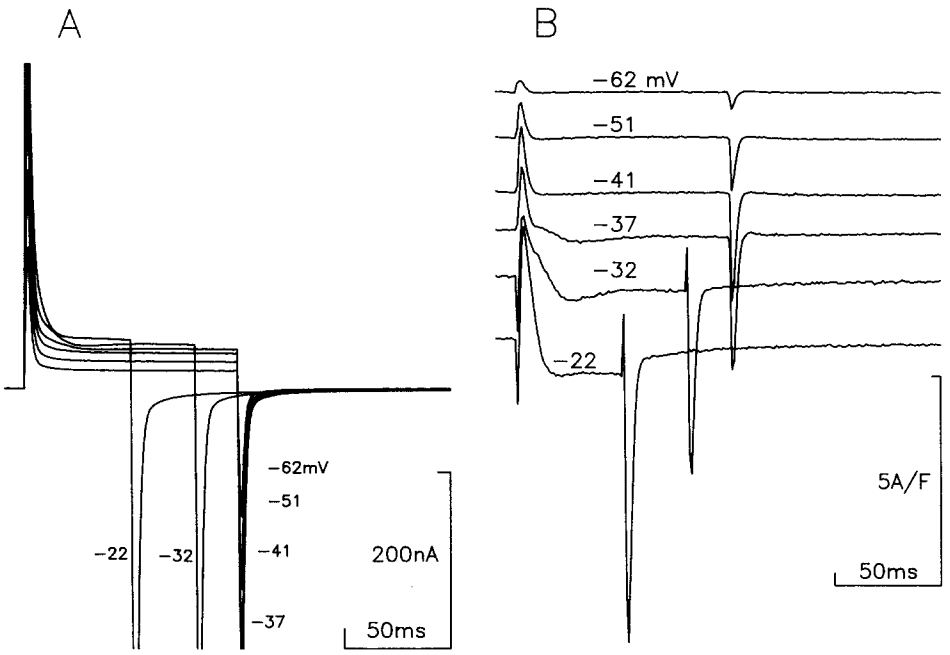

FIGURE 7. An inward phase in membrane current. (*A*) Total currents during 100-ms pulses (from a h.p. of −80 mV) to the voltages indicated. (*B*) Asymmetric currents, differences of records in *A* minus a scaled control (20 mV from −100 mV). All records are single sweeps. The control is the same for all 100-ms pulses. Fiber 644. External solution, 10 Ca. Internal solution, 15 EGTA. Linear capacitance, 14.7 nF. Diameter, 80 μm. Slack fiber, sarcomere length not measured. Temperature, 16°C.

Initially we attributed this inward-going phase to either an inward ionic current that activates and inactivates during the pulse, or to a slow activating outward current. We ruled out these explanations on the following grounds: (*a*) The inward current was observed with a variety of cation channel blockers in the extracellular medium, including Cd, Co, La, Mg, TEA, diaminopyridine, and TTX. (*b*) Inward phases were observed both in the presence and in the absence of the anion channel blocker A9C, and with or without EGTA in the internal medium. (*c*) In four

experiments we confirmed the observation in Fig. 7 that its amplitude is voltage-dependent and goes through a maximum at about the voltage that makes the hump most noticeable. These results are presented in Fig. 8. The amplitude of the inward-going phase was measured in the asymmetric membrane current as the difference between the minimum and a final level found by averaging the current during the last 40 or 10 ms of the ON (for 100- and 50-ms pulses). These amplitudes are plotted in the figure as a function of test voltage. They reach in all cases a well-defined maximum at intermediate voltages. (*d*) The inward phase is associated with E-C coupling, as is the outward hump. The symbols above the frame of the graph in Fig. 8 mark the minimum voltage that elicited intrinsic optical signals in each fiber. This threshold is always a few millivolts negative to the voltage that elicits the maximum inward phase. (*e*) All interventions that reduced the hump simultaneously reduced or eliminated this inward phase, as exemplified in Fig. 2 of this paper, Fig. 17 of Csernoch et al. (1991), and Fig. 6 of Szűcs et al. (1991). Fig. 4 of

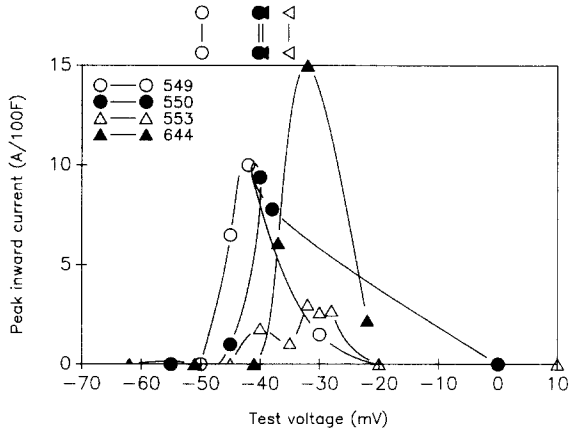

FIGURE 8. Voltage dependence of the inward phase. Amplitude of the inward phase in the asymmetric current, measured between negative minimum and average of the last 50 ms (for 100-ms pulses) or 5 ms (for shorter pulses). The symbols above the frame of the graph mark the voltage at which an intrinsic absorbance signal was first seen. All fibers were at slack length, with internal solution 15 EGTA and no dye. The external solution was 10 Ca for 644 and Co-Ca for all others. Linear capacitance (in nF, in order of increasing fiber numbers): 19.6, 22.2, 17.0, and 14.7. Temperature, 16°C for 644, and 12–14°C during the other experiments.

Szűcs et al. (1991) illustrates a converse effect. Caffeine increases the hump and a small inward phase at contractile threshold and at 5 mV below threshold.

The properties listed make it unlikely that this phase is due to the inward movement of cations. It is still possible that an anionic current could explain all the properties. The inward phase, however, has the property of conservation of charge in ON and OFF transients, a characteristic generally inconsistent with ionic currents.

Fig. 9 and Table I illustrate this property. The experiment in Fig. 9 is representative of four analogous experiments in which pulses of different duration were applied, all at a voltage that generated an asymmetric current with a large inward phase. The durations were chosen to intersect the inward phase at various times. Signal averaging was used to improve the measurement of areas. The speed of the voltage clamp was slowed (by increasing a lead capacitance in the feedback circuit; Brum and Ríos, 1987) to reduce errors of measurement in the first millisecond of the pulses.

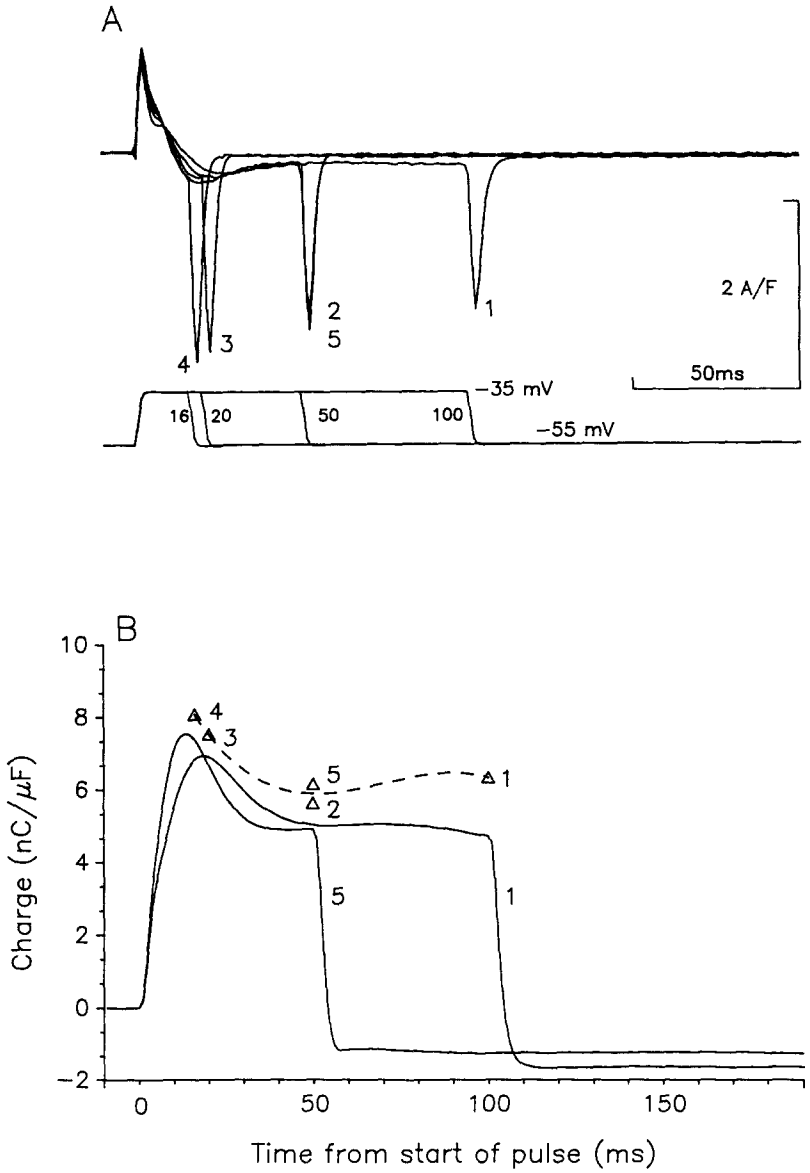

FIGURE 9. Conservation of charge in the inward current. (*A*) Asymmetric current during pulses of different duration; records of $V(t)$ are at the bottom of the panel. h.p. = −85 mV. Controls 20 mV from −85 mV. Averages of two sweeps separated by 150 s. The averages were obtained in the order indicated by numbers next to each record. (*B*) Lines are running integrals of records 1 and 5 at top, after subtraction of baselines. The OFF baselines were fitted from 51 ms after the end of the pulse to the end of the record. At the ON, a baseline was fitted to record 1 between 51 and 100 ms. Record 5 was corrected by subtraction of the average level at the last 5 ms of the ON. The triangles represent the OFF charges for every record in A. Fiber 643. External solution, 10 Ca. Internal solution, 15 EGTA. Controls, 20 mV from −90 mV. Linear capacitance, 17.7 nF. Slack fiber, diameter and sarcomere length not measured. Temperature, 16°C.

The top panel shows the asymmetric currents elicited by pulses to −35 mV from a prepulse level that was subthreshold for this fiber ($V(t)$ records at bottom of panel). The asymmetric currents have a visible hump followed by a negative phase that lasts until ~50 ms. Pulses shorter than 50 ms produced substantially greater OFFs, as expected if they interrupt the return of mobile charge during the ON. The records are numbered in the order in which the pulses were applied. The sequence took 35 min to complete, and the kinetics of hump and inward phase changed somewhat during this time. The pulse at 50 ms was repeated at the end of the sequence and moved approximately the same amount of charge as the first pulse of the sequence, as shown in the bottom panel.

The bottom panel is a comparison of the running integrals of records 1 and 5 (curves) with the OFF areas of all five records (triangles). Before calculating the

TABLE I

ON and OFF Charges For Two Pulse Durations

1	2	3	4	5	6	7	8	9	10
Fiber	Voltage		Q (20 ms)		Q (50 ms)		4–6	5–7	
No.	pre	test	ON	OFF	ON	OFF	ON	OFF	Solution*
	mV	*mV*	*nC/μF*		*nC/μF*		*nC/μF*	*nC/μF*	
572	−55	−30	10.9	11.0	9.7	8.0	1.2	3.0	Cd-La-9AC
615	−70	−45	8.6	7.7	4.9	5.2	3.7	2.5	Reference
621	−65	−50	4.9	5.7	3.7	3.8	1.2	1.9	10 Ca
643	−55	−35	7.2	8.1	5.2	6.1	2.0	2.0	10 Ca
Average							2.02	2.35	
SEM							0.68	0.29	

ON charge at 50 ms (column *6*) was determined by integration of asymmetric current during a 50-ms pulse, after subtraction of the average level during the last 10 ms of the ON. ON charge at 20 ms (column *4*) was determined from the running integral of charge movement in the 50-ms pulse. OFF charges (columns *5* and *7*) were determined on 20- and 50-ms duration pulses to the same voltage after subtraction of a baseline fitted from the 71st ms to the 145th ms after the end of the pulse. Column *8* lists the differences between values of ON charges. Column *9* lists the corresponding differences in OFF charge. Capacitance in control currents (in nC/μF): 2.2, 25.2, 9.5, and 17.7. Diameters (in μm): 68, 131, 59, and 50. Temperature (in °C): 14, 12, 12, and 16.

*Composition of solutions given in Table I of Csernoch et al. (1991).

running integrals, records 1 and 5 were corrected for small ionic currents, visible in the traces, as explained in the figure legend.

The running integrals go through a peak and then decrease sharply during the ON, as obviously expected. More interestingly, the OFF areas (triangles) reproduce this decaying trend as the duration increases. The OFFs are always somewhat greater than the running integrals. The small but systematic differences could be due to errors in the correction for ionic current or to asymmetries in the controls. In spite of these imprecisions, the result agrees with a capacitive nature of the inward current.

Table I collects results from four experiments, including the one illustrated. Listed are the prepulse and test pulse voltages (which were determined independently in each experiment to optimize the size of the inward component), the charges at 20 and 50 ms for both ON and OFF, and their differences. In all cases the ON area at 20

ms was determined from the running integral of the charge movement current during the longer pulse. The table shows that the running integrals of both the ON and the OFF charges were significantly greater at 20 ms than at 50 ms. The difference could be as much as 40% of the total charge moved in the 20-ms pulse. The excess charge moved by the short pulse was 2 or 2.35 nC/μF (at ON and OFF), which is therefore our estimate of the charge that moves inwardly during the pulse (in this sense the result of Fig. 9 is typical). Though different at both durations, the total charge movement was on average about equal at ON and OFF.

The sum of the evidence in this section indicates that the inward component frequently seen in the asymmetric current is capacitive in nature. The movement of inward capacitive charge during a depolarizing pulse is illuminating regarding possible models: it is difficult to explain, unless the usual assumption of constancy of transmembrane potential during the pulse is abandoned. Since this inward component is associated with the hump and is suppressed or reduced together with the hump, it is probably originated by a similar mechanism. A specific mechanism that may generate both a hump and an inward phase will be considered in the next section.

DISCUSSION

The first two papers of this series and the results in this paper show that four interventions, protocol 1, depletion, ruthenium red, and 20 μM tetracaine, inhibit the Ca release process and suppress a current that was identified kinetically with the hump. It is highly likely that the release process is the primary target of the first three interventions. In the third paper, the SR release agonist caffeine was shown to shift the contractile threshold to lower voltages and cause the appearance of a current with similar characteristics at potentials that were below the contractile threshold in the absence of the drug but suprathreshold in its presence. Since this effect was virtually opposite to that of tetracaine, it was suggested that the primary target of tetracaine (at 25 μM) is also the SR.

The current suppressed by these interventions (promoted in the case of caffeine) was termed I_γ on the basis that it includes the hump component in the asymmetric current. Unlike classical definitions of I_γ (Huang, 1982; Hui, 1983*a*, *b*), this definition resulted in a current with a negative phase after the hump. This negative phase in the difference may result from the suppression of an actual inward current or a slowing of an outward current, which results in a negative phase present only in the difference record.

In this paper we have taken advantage of the convenient protocol 1 to study the voltage dependence of I_γ, and have found this dependence to be bell-shaped, decaying at high voltages. We also found this to be the case for the current suppressed by 20 μM tetracaine.

This finding is not consistent with the idea that I_γ and I_β are carried by different molecular species, undergoing parallel transitions. An independent species of charge cannot generate a current with nonmonotonic voltage dependence if it moves under the sole influence of a constant applied field. The rate of the transition, and thus the intensity of current, are only expected to increase at higher voltages.

Additionally, such current cannot have a negative phase upon depolarization. The simple concept that a passive charge can only move down the electric field is shown to hold in very general systems by Duane and Huang (1982). They showed in general that multiple systems of mobile charges, each with multiple states, all contribute positive terms to the capacitance, meaning that each of them contributes positive current upon depolarization.[2]

Thus, the observation of inward current during the ON is puzzling, and it becomes important to demonstrate that this current is indeed capacitive. We ruled out an ionic nature of this current for several reasons: insensitivity to anion and cation channel blockers, correlation with the magnitude of the hump, bell-shaped dependence with membrane potential that reaches a maximum at potentials close to those that make the hump most noticeable, multiple correlations with E-C coupling, including the fact that the maximum occurs at voltages slightly above the threshold for Ca^{2+} release, and the reduction or elimination of this current by interventions that reduce Ca release flux (and the hump).

One of our referees suggested the interesting possibility that this inward current might be calcium activated, which would explain its tight association with E-C coupling. This is unlikely for the reasons given above that rule out an inward cationic current, plus the apparently greater amplitude in the presence of high intracellular concentrations of EGTA. Additionally, the magnitude of a calcium-dependent current would not be expected to decay above −40 mV. Most important, the charge moved in the OFF transient depends on the duration of the pulse, as expected if the inward phase is capacitive (Fig. 9 and Table I).

A Model of I_γ

It is possible to explain both the hump and an inward phase of charge movement with the model introduced in the first paper of this series. The model assumes that Ca^{2+}, at an elevated myoplasmic concentration near the release sites, increases the effective transmembrane potential by electrostatic screening of, or binding to, negatively charged sites on the myoplasmic face of the T membrane. Having at hand simultaneous records of I_γ and Ca release flux, we could test these ideas quantitatively, with definitively favorable results.

To generate a quantitative version of the model we had to decide first whether the change in transmembrane potential caused by Ca^{2+} binding would be local, affecting only the intramembranous voltage sensors (as would be produced by Ca^{2+} binding to specific proteins), or widespread, altering the potential over the entire membrane surface (as expected from binding to membrane lipids). An apparent consequence of the first alternative is that only the nonlinear charge would respond to the extra potential. In the second case, the extra potential would result in extra movement of nonlinear plus linear charge, with consequent major differences in voltage distribution and kinetics.

The first possibility was chosen as it accounts readily for the nonmonotonicity of

[2] They had to assume that terms of higher order than the first are negligible in an expansion of the free energy of the system in powers of the transmembrane potential.

the voltage dependence (Figs. 4–6) as follows: a suprathreshold depolarizing pulse to a low or intermediate voltage (e.g., −40 mV) will cause some movement of Q_β and open some release channels. The released Ca^{2+} will bind to negatively charged sites on or near other voltage sensors, causing them to undergo the activation transition and thus causing I_γ (the delayed hump). At greater depolarizations, causing near-maximal movement of Q_β and Ca release, there will still be neutralization of negative charges by Ca^{2+}, but the extra potential will not cause additional charge movement as the greater pulse potential has already caused the charge-moving transition in most of the sensors. If this binding of Ca^{2+} caused substantial movement of linear capacitive currents, the I_γ current would not decay but would increase at high voltages. Thus, the "local" version of this model is chosen in principle.

A complicating issue is that any change in surface potential, local or widespread, will cause some movement of linear charge; that is, the movement of extra linear charge will always accompany intramembranous charge movement caused by ion binding. This linear contribution, however, is small. In Appendix I we calculate in general the linear capacitive charge that moves when ions bind to the internal membrane surface, and apply the result to a hypothetical case in which one Ca^{2+} ion is assumed to bind to every sensor (assumed at a density of four per junctional foot complex). The linear current that flows in this case is shown to be very small.

Fig. 10 represents the model chosen for generation of I_γ. The voltage sensors have sites bearing negative charge on their myoplasmic face. They undergo transitions (between two states) driven by the "microscopic" or local transmembrane potential, the difference between the electric potential at the two faces of the membrane.

Fig. 10 *B* is a plot of the electric potential along a coordinate perpendicular to the plane of the membrane. As shown, the microscopic transmembrane potential (V_m^*) is determined by the macroscopic or bulk potential difference (V_M) and to two surface potential terms. V_{se} represents the external surface potential (unknown and constant). The inner surface potential will vary according to the occupancy of the binding sites by Ca^{2+} in a range between two extreme situations: the resting situation, essentially Ca free, in which the negative potential is maximum, and the saturated situation, in which it will have a value V_{si}. We term V_{max} (a negative quantity) the difference in surface potential between these extremes. If $p(t)$ represents the occupancy of the sites at time t, the microscopic transmembrane voltage will be

$$V_m^* = V_M + [1 - p(t)]V_{max} - V_{se} + V_{si} \tag{2}$$

There is no way in the model to specify V_{si} and V_{se}; V_m^* is therefore unknown, but the term

$$V_m \equiv V_M + [1 - p(t)]V_{max} \tag{3}$$

is all that is necessary for the calculations. The diagram in Fig. 10 *C*, which includes only the terms in Eq. 3, illustrates this simplication. The two plots of electric potential shown correspond to the situations before and after binding of an amount of Ca^{2+} that causes partial saturation of the sites S. The simple reaction scheme chosen for these sites is also represented in *C*. The model thus requires three parameters: two kinetic constants and V_{max}.

Simulations: Kinetics of the Binding Site

To actually simulate I_γ three steps are necessary: (*1*) Estimate the time course of $[Ca^{2+}]$ in the myoplasm near the T-SR junction. We term this the "triadic Ca transient" ($[Ca^{2+}]_T(t)$) and estimate it using a diffusion model of a sarcomere in which

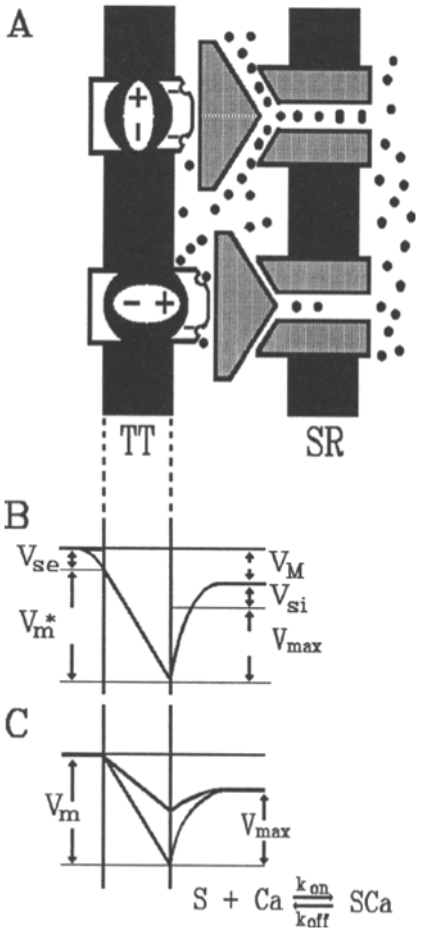

FIGURE 10. Model for the generation of I_γ. (*A*) Cartoon showing two sensor–channel pairs. The top one is activated (sensor has undergone its activating transition, release channel is open) and Ca^{2+} is flowing into the myoplasm. Ca^{2+} binds to sites on the myoplasmic face of both sensors and increases the transmembrane potential to a value less negative inside. This increase may cause other sensors, like the one at the bottom, to undergo the activating transition, causing the delayed current, I_γ, and further channel opening. (*B*) Diagram of potential across the membrane. The microscopic transmembrane potential difference V_m^* is the result of several additive terms (Eq. 2), including a bulk potential difference (V_M) and surface potential terms. The internal surface potential is negative, and may be reduced (made smaller in absolute value) by binding of Ca^{2+}. V_{max} is the maximum surface potential that may be offset due to Ca^{2+} binding. The total internal surface potential is the sum of V_{max} and a Ca^{2+}-insensitive term, V_{si}. V_{se} is the surface potential at the extracellular face. (*C*) Simplified version of the potential profile, in which the Ca^{2+}-insensitive terms V_{si} and V_{se} have been omitted. The potential profile at the bottom represents the resting situation, when the negative sites are free of Ca^{2+} and make their full contribution to the surface potential. The top profile represents the effect of an increase in $[Ca^{2+}]$, which determines occupancy of a fraction of sites in a reaction represented at the bottom of the figure.

Ca is released at both ends and diffuses toward the middle while binding and removal take place. Binding and removal are computed using parameters fitted independently in the process of determining Ca release flux. Therefore, for the purpose of the simulation of I_γ, the parameters of binding and removal are fixed. The details of

the diffusion calculations are given in Appendix II. The outcome is one triadic Ca transient $[Ca^{2+}]_T(t)$ for every depolarizing pulse.

(*2*) Use the calculated $[Ca^{2+}]_T$ to drive a binding reaction of Ca^{2+} to the negatively charged site S. This generates the occupancy function

$$p(t) \equiv \frac{[CaS]}{[S]_{total}}$$

where the values of $[S]_{total}$ and [CaS] are unknown.

(*3*) Use Eq. 3 to determine the microscopic transmembrane potential $V_m(t)$. $V_m(t)$ is then used to drive transitions in an ensemble of charged molecules with two states, the equilibrium of which obeys the (Boltzmann) canonical distribution equation

$$Q(V) = Q_{max}/[1 + \exp[-(V_m - \overline{V}_m)/k]] \tag{4}$$

The kinetic constants of the ensemble, k^+ and k^-, are exponentials of second order functions of voltage (a description introduced by Simon and Beam [1985] that fits the kinetics of I_β at high voltages well and was also used by Brum and Ríos [1987] in their description of charge 2):

$$\begin{aligned} k^+(V_m) &= \alpha \exp\{(V_m - \overline{V}_m)/2k - 0.15[(V - \overline{V}_m)/2k]^2\} \\ k^-(V_m) &= \alpha \exp\{-(V_m - \overline{V}_m)/2k - 0.15[(V - \overline{V}_m)/2k]^2\} \end{aligned} \tag{5}$$

where $\alpha = k^+(\overline{V}_m) = k^-(\overline{V}_m)$. This generates the charge movement currents.

All three steps require the specification of model parameters, namely, diffusion and binding parameters for step 1, V_{max} and the kinetic constants of binding and dissociation for step 2, and equilibrium and kinetic parameters of charge movement in step 3. Of these, only the parameters of steps 2 and 3 are adjustable to fit the data. The removal parameters for step 1 are fitted independently to satisfy the kinetics of the Ca transients (Brum et al., 1988*b*).

For step 2 it is necessary to establish the affinity of the binding sites for Ca^{2+} and a kinetic constant. An experiment was devised to determine the speed of dissociation from the site. The threshold depolarization to elicit Ca^{2+} release was determined within a 5-mV range, which was defined with two 100-ms pulses such that the highest one elicited a visible change in absorbance (judged after the pulse on the digitized optical record at 720 nm wavelength) and the lowest one did not. Then a relatively large conditioning pulse was applied and the threshold was determined again with pulses applied 150 ms after the conditioning. Had the binding of Ca due to release during the conditioning pulse persisted for the intervening 150 ms, the threshold would have been lowered. Three experiments (not shown) had a negative result: no change in the threshold was observed. In the framework of the model the OFF rate from the site is fast enough that in 150 ms the occupancy is back to resting level. The OFF rate constant of the Ca^{2+}:S binding reaction (k_{off}) should therefore be several-fold greater than 10 s^{-1}. Additionally, the close relationship observed by Csernoch et al. (1991) between $\Delta I_1(t)$ and $\ddot{R}(t)$ can be explained with this scheme, but only if the site is fast, as discussed in the first paper.

The dissociation constant K_{dCaS} was set by trial and error, based on the success of the simulations presented later, at 16–20 μM in three fibers simulated in detail. If the

ON rate constant is close to the diffusion limit, or $\sim 10^8$ M^{-1} s^{-1}, the k_{off} will be $\sim 2{,}000$ s^{-1}. These values were used in the calculations, and they imply that the sites are in equilibrium with Ca^{2+} in the time scale of interest. Although the simulations were carried out using the kinetic equations, an assumption of instantaneous equilibrium should give the same results.

The parameters of charge movement have to satisfy the kinetics and voltage dependence of I_β, since in the model there is only one set of charged particles. Their values were established by trial and error, trying to reproduce both the fast phase and the hump at the ON as well as the OFF of the asymmetric current, and the simpler kinetics of the asymmetric currents after conditioning. Fig. 16 compares the asymmetric currents of experiment and model. As remarked below, for a kinetically accurate simulation it was necessary to assume a rate of charge movement greater than expected.

Detailed simulations for the experiment illustrated in Figs. 2–4 are shown for all records in Figs. 11–16. Fig. 11 plots the release fluxes derived from the Ca^{2+}

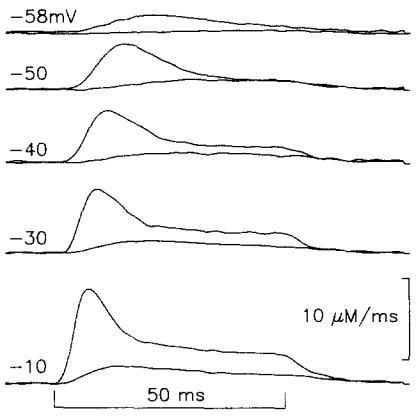

FIGURE 11. Ca release flux and protocol 1. The records of $[Ca^{2+}](t)$ represented in Fig. 3 and other records not shown were digitally filtered and fitted with the removal model of Brum et al. (1988*b*; also described in Csernoch et al., 1991) and used to derive records of Ca release flux by the method of Melzer, Ríos, and Schneider (1984, 1987). The parameter values used are listed in Table II. Represented are the release fluxes corresponding to all the records in Fig. 3. In all cases the top record is reference and the bottom record is conditioned.

transients shown in Fig. 3. Digital filtering as described and illustrated in Fig. 3 was used before the computation of release flux. The records of release are very similar to the Ca^{2+} transients; this was also noted by García et al. (1991). As argued by Ríos et al. (1990), this is a consequence of the assumption of slow kinetics of Ca^{2+} binding to EGTA (Smith et al., 1984), which, at ~ 8 mM inside the cell, accounts for most of the removal flux.

Fig. 12 shows the $[Ca^{2+}]_T(t)$ records (triadic Ca^{2+} transients) obtained from the release records in Fig. 11 (with diffusion calculations described in detail in Appendix II). As expected from the argument made by Csernoch et al. (1991), the time course of these triadic Ca^{2+} transients is similar to that of release flux (the $[Ca^{2+}]_T$ waveform is only slightly delayed and decays somewhat more slowly).

Fig. 13 illustrates step 2. Given the assumption of fast equilibration and relatively low affinity of the Ca^{2+}-binding sites, it follows that the occupancy of the sites ($p(t)$) will have a time course very similar to the $[Ca^{2+}]_1(t)$ in Fig. 12. These occupancies

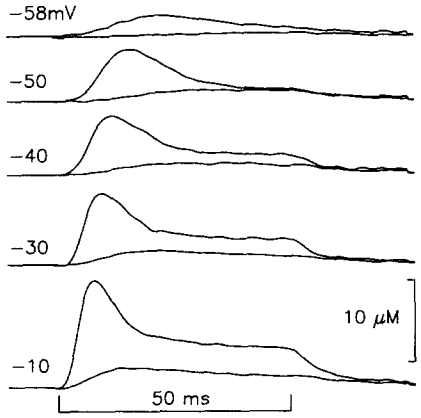

FIGURE 12. $[Ca^{2+}](t)$ near the triads. The model of diffusion described in Appendix II was used to derive the time course of Ca^{2+} concentration in a small region near the sites of release. The parameters used in the simulation of diffusion include the parameters of removal (Table II) and the diffusion coefficient of Ca^{2+} in myoplasmic water, 2.8×10^{-6} cm^2 s^{-1}.

(not shown) were used to compute the microscopic transmembrane potential V_m (Eq. 3) equal to the clamp potential plus the term $[1 - p(t)]V_{max}$ (constituting the "hump"). The scale in the figure refers to the microscopic potential, and the number next to each pair of records is the clamp potential during each pulse. Initially the microscopic potential is −100 mV (equal to the clamp prepulse, −70 mV, plus V_{max}, −30 mV). During the pulse the voltages have humps in reference but not in conditioned records. The highest value of voltage reached during the largest pulse is about −25 mV, which is 15 mV more negative than the clamp voltage, indicating a maximum occupancy of ~50% for this set.

The close relationship between $\ddot{R}(t)$ and $I_\gamma(t)$ reported in the first paper can be understood in principle considering these voltages. A capacitive current driven by these voltages will be roughly proportional to their time derivative, which in turn is close to the time derivative of the release flux $\dot{R}(t)$.

Fig. 14 represents the result of step 3. Shown are the charge movement currents generated by the voltages in Fig. 13 acting on an ensemble of two-state voltage

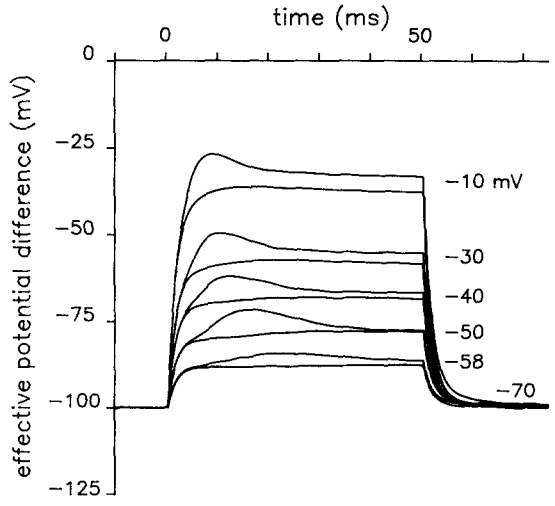

FIGURE 13. Microscopic voltages. Records of $V_m(t)$ in reference and conditioned pulses to the potentials indicated. Calculated from the $[Ca^{2+}]_T(t)$ records in Fig. 12, which were used to drive a binding reaction to the hypothetical negative sites. The fractional occupancy $p(t)$ was then used in Eq. 3 to derive the microscopic transmembrane potential difference $V_m(t)$. Parameters are listed in Table II (fiber 612).

sensors (Eqs. 4 and 5). The four parameters describing the ensemble are listed in Table II and were found by trial and error, judging primarily from the success in the description of I_γ as a function of both time and voltage. The choice of parameters also resulted in a reasonable simulation of the fast phase before the humps.

Fig. 15 illustrates the simulated $I_\gamma(t)$ records (thicker traces), obtained as differences between reference and conditioned currents in Fig. 14. The simulated records have all the qualitative properties of I_γ found in the experiments, including a large hump at the ON, a negative phase after a hump, a small OFF that becomes biphasic at high voltages, and the bell-shaped voltage dependence of the current amplitude, illustrated for experimental records in Fig. 6.

The anomalous kinetic aspects of I_γ can now be explained. That the phenomenon occurs at the ON and is small and variable at the OFF is a consequence of the waveform of Ca release flux, which has a large early peak followed by a decay to a much lower level. The simulated waveform of triadic $[Ca^{2+}]$ (Fig. 12) has a similar

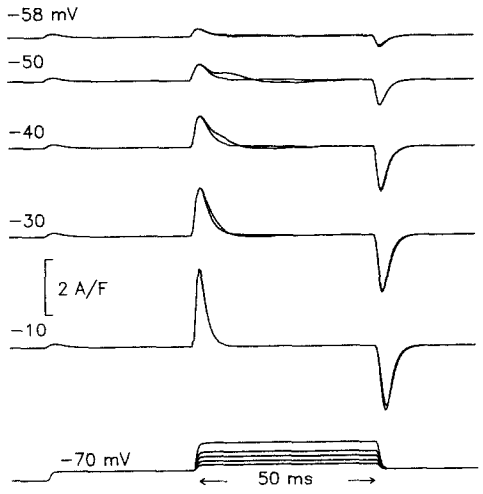

FIGURE 14. Simulated charge movement currents. Currents caused by the voltages in Fig. 13 in an ensemble of charged particles undergoing transitions between two states. The properties of the ensemble are given by Eqs. 4 and 5. The parameters are listed in Table II. These records should be compared with the records in Fig. 2 and are plotted at the same scale.

peak followed by a decrease during the ON. This marked increase in $[Ca^{2+}]$ causes a marked increase in occupancy and local voltage (Fig. 13) driving the positive or outward phase of I_γ (Fig. 15). The peak in $[Ca^{2+}]_T$ is followed by a decrease, and a corresponding decrease in local voltage. This decrease in local voltage during the ON in turn causes an inward movement of charge.

Fig. 15 also plots the experimental $I_\gamma(t)$ (that is, the records of Fig. 4) at the same scale. This permits us to judge in detail the result of the simulation. The kinetics of the ON are generally well described, including size and shape of both phases at all voltages except −10 mV. The amplitude of the current, defined as the difference between maximum and minimum, is essentially correct at all voltages in the simulation. The time to peak of the simulated records is within 2 ms of the experimental value at all voltages. The simulation of the OFF, however, is less successful: the change in polarity observed at high pulse potentials in this and several

other experiments is present in the simulations, but the amplitude of the OFF transients is underestimated at all voltages.

Some of the inadequacies in the simulation may be due to errors in the experimental records, like the presence of ionic current (especially at −10 mV), charge 2 (Brum and Ríos, 1987), and movements of charge under the Vaseline seals

TABLE II

Model Parameters

A. Parameters of Removal.

Fiber No.	$k_{OFF,MgP}$	M	[P]	$k_{OFF,CaP}$	$K_{d,Pp}$	[EGTA]	$K_{OFF,CaEGTA}$	Temp.
	s^{-1}	s^{-1}	μM	s^{-1}	μM	mM	s^{-1}	°C
612	3	1,000	1,000	1	1	8*	1.25	13
574	3	200	100	1	1	4	0.5	15
493	4.7	633	375	0.9	1.9	0.1‡	‡	13

B. Parameters of Binding.

Fiber No.	$K_{d,CaS}$	V_{max}
	μM	mV
612	16	−30
574	20	−20
493	20	−20

C. Parameters of Intramembranous Charge.

Fiber No.	Q_{MAX}	V	k	α
	$nC/\mu F$	mV	mV	ms^{-1}
612	14	−74	11	0.25
574	35	−50	15	0.15
493	25	−50	15	0.2

Parameters of removal were determined by fitting the removal model (Brum et al., 1988*b*) to the OFF phases of multiple Ca^{2+} transients in the same experiment. All parameters listed were allowed to be changed by the fitting routine in at least one of the fibers; parameters were not allowed to change and their set values are listed below. For fiber 574 a fit could not be obtained with [EGTA] set at 8 mM, the concentration in the end pools, but a good fit was obtained with the lower concentration listed. Parameters of Ca^{2+} binding to a hypothetical site and parameters of charge movement were chosen by trial and error to optimize the simulation of $\Delta I_1(t)$ and $\Delta I_a(t)$ as described in the text. Symbols: $k_{OFF,MgP}$, off rate constant of Mg:parvalbumin; $k_{OFF,CaP}$, off rate constant for Ca:parvalbumin; M, maximum pump rate; $K_{d,Pp}$, dissociation constant for Ca^{2+} on pump sites; $k_{OFF,CaEGTA}$, off rate constant of Ca:EGTA. $K_{d,CaS}$, dissociation constant of the Ca^{2+}:membrane site binding reaction. Other symbols as in text. Other parameters were set, and their values were, in all cases: $k_{ON,CaEGTA}$, 1.25 $\mu M^{-1}s^{-1}$ (Smith et al., 1984); $k_{ON,Catroponin}$, 125 $\mu M^{-1}s^{-1}$; $k_{ON,CaP}$, 100 $\mu M^{-1}s^{-1}$; $k_{ON,MgP}$, 0.03 $\mu M^{-1}s^{-1}$; $k_{OFF,Catroponin}$, 1,200 s^{-1}; [troponin], 240 μM; [Ca^{2+}], 0.01 μM (in high EGTA experiments) or 0.05 (in fiber 493); [Mg^{2+}], 900 μM; $k_{ON,CaS}$ (ON rate constant to the membrane sites), 125 $\mu M^{-1}s^{-1}$.

*[EGTA] was set equal to the concentration in the end pools.

‡EGTA was neglected in the removal fit.

(Hui and Chandler, 1990). We believe, however, that these sources of error do not alter the qualitative aspects of I_γ described in these papers, all of which are well reproduced in the simulations.

Fig. 16 compares the simulated charge movement currents with the experimental asymmetric currents of Fig. 2. The main discrepancy is the existence of a slow inward

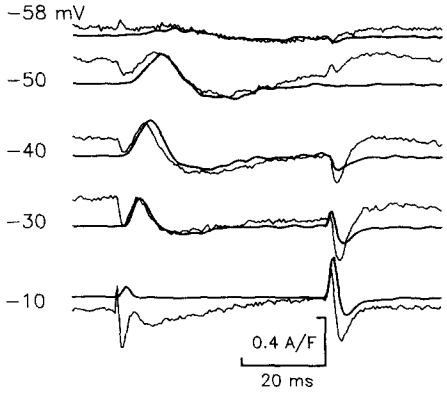

FIGURE 15. I_γ in the simulation. *Thick traces,* Differences (reference minus conditioned) between simulated records of Fig. 14. *Thin lines,* Experimental records (same as in Fig. 4). The records were shifted vertically to facilitate the comparison of amplitudes but were not scaled.

phase in all the experimental records, at both ON and OFF, which continues to increase during the pulse and is not present in the simulations. The fact that this phase is net inward is an indication that it may be due to asymmetric ionic currents. It should not have any relationship with the activation of Ca^{2+} release as the peak of release occurs very early in the pulses. Consequently, when trying different parameter values in the simulation, we opted for values that reproduced well the early peak and the hump, rather than this late phase. This phase was small or nonexistent in another fiber studied in detail (cf. below).

Table II gives values of parameters used to simulate records in two other fibers. #574 is a slack fiber with high EGTA, and #493 is a stretched fiber with low EGTA. The fits for these fibers were also reasonable. In the asymmetric currents of #493 (not shown) the slow net inward phase described in Fig. 2 was not present; the $\Delta I_1(t)$'s were, however, of smaller amplitude, as is usual with stretched fibers. The parameters of removal are within the values found in previous work (for instance in Table II of Csernoch et al., 1991). Similar parameters of the binding site were found to be

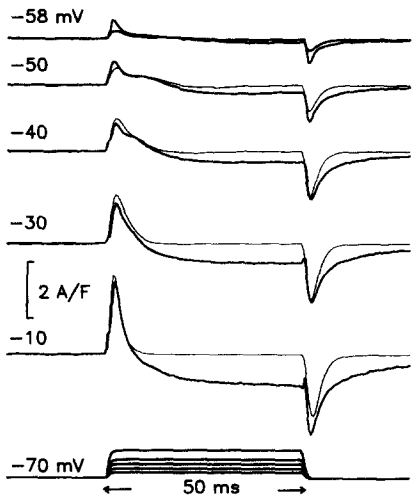

FIGURE 16. Asymmetric currents in theory and experiment. Simulated records (*thin lines*) from Fig. 14, reference only, and corresponding experimental asymmetric currents (*thick traces*) from Fig. 2. The records are shown on the same scale.

suitable in the three fibers. The central voltage of the charge distribution ($\overline{V}_m$)is negative by comparison with published values, and it should be, as it is a microscopic potential, shifted from the bulk potential by V_{max} (cf. Fig. 13).

The kinetic parameter α, equal to half of the rate constant of charge movement at the central potential (Eq. 5), was between 0.15 and 0.25 ms^{-1}. Simulations with α less than 0.1 ms^{-1} resulted in I_γ transients slower than the experimental $\Delta I_1(t)$ records in all three fibers. These values are much greater than the value measured by Hollingworth and Marshall (1981) in intact frog sartorius fibers at 15°C (0.05 ms^{-1}). They are closer to values reported in mammalian fibers at 15°C by Simon and Beam (1985) and smaller than the values suggested by Lamb (1986*a*) from observations on the effects of hypertonic solutions.

The fast kinetics that must be assumed to make the model fit casts doubt on the validity of the model. However, it is possible to explain the high values for α required in our simulations with the suggestion by Lamb (1986*a*) that the kinetics of charge movement currents are slower than the intrinsic kinetics of the sensors due to cable delays in the T tubules. Indeed, a slow charging of the T tubules should affect the kinetics of I_β but not of I_γ, as the mechanism proposed for I_γ involves local charges. In other words, the characteristic RC values that determine the charging delays are much smaller for I_γ, as the capacitance involved does not include the linear capacitance of the T membranes (cf. previous description of general aspects of the model).

The mechanism proposed here brings into focus a property of I_γ overlooked until now: when seen in a record of total charge movement current, the hump has both a delayed onset and a rapid termination. These two kinetic features of the ON are visible in many published records. The rapid termination is explained by our theory as a consequence of an actual movement back, or inward, of the charge carriers. Considering the role of these charge carriers as voltage sensors, this could have physiological importance as a mechanism to hasten the decay of release after the peak.

The main regulatory consequence of the present mechanism, however, is one of positive feedback: Ca^{2+} release will cause I_γ, I_γ will open more release channels, and this will increase Ca^{2+} release. Some experimental observations consistent with the operation of this process have been communicated (Pizarro et al., 1990).

Comparisons with Previous Work

The existence of at least two components in the charge that moves upon depolarization of resting fibers was first noticed as separations from simple exponential kinetics (Almers, Adrian, and Levinson, 1975), as separations from simple sigmoidal voltage dependence (Adrian and Almers, 1976), and as a component more susceptible to voltage-dependent inactivation (Adrian and Peres, 1979). The term Q_γ was coined by Adrian and Peres (1977) to name these delayed components, and a large body of work on this component ensued.

In view of this vast literature, we will only consider here the aspects of the previous publications that conflict with the present work and have resulted in the "γ sensor" view (that Q_β and Q_γ result from different voltage sensing systems operating in parallel; reviewed by Huang, 1989). We will not consider studies on mammalian

muscle, in which Q_γ manifests itself as a tetracaine-sensitive component (Lamb, 1986*b*) but is very difficult to identify kinetically (Hollingworth, Marshall, and Robson, 1987, 1990).

The studies of Q_γ can be classified in four classes, and the comparisons with the present results will be carried out in the same order:

Kinetic Studies

These include kinetics of the ON and OFF (Hui, 1983*b*; Huang, 1984), modification of kinetics by prepulses (Adrian and Huang, 1984*a*) or drugs (Huang, 1987), and effects of temperature on kinetics (Hui, 1991).

The present papers add to the known kinetic features of I_γ the observation of an inward phase during the ON. This phase had not been noticed before, probably because the inward phases are very clear only in high intracellular [EGTA], particularly in unstretched fibers, and most of the published studies of kinetics were on intact fibers in hypertonic solutions. Inward phases during the ON were observed by all three laboratories involved in the present series. In addition, recent work by Heiny, Jong, Bryant, Conte Camerino, and Tortella (1990) has also produced records with inward phases during the ON. Inward phases of I_γ can be found in the earlier literature if one subtracts asymmetric currents in tetracaine from the corresponding reference records (for instance, records in 1.5 mM tetracaine in Fig. 10 of Hui, 1983*a*).

The published reports that deal with OFF kinetics of I_γ are contradictory. In a detailed study Huang (1984) concluded that Q_γ has rapid, monophasic OFFs even at voltages near the midpoint of its distribution, with time constants in the 10–15-ms range. This is, however, inconsistent with other work of Huang and collaborators (Csernoch, Huang, Kovac and Szűcs, 1987), in which heavily averaged difference records (reference minus tetracaine) show a clear bell-shaped ON and no visible transient at the OFF. This is also in contrast with the observations of Hui and Chandler (1988) of two kinetic components, one fast and one slow (presumably I_γ), in a stepped-off study of Q_γ. In the present series of papers the OFF of I_γ is generally much smaller than the ON and in some cases negligibly small. This is consistent with our model (Fig. 14), which also predicts larger and inverted or biphasic OFF transients at higher test voltage. Inverted and biphasic OFFs at high voltage were found experimentally (Fig. 17 in Csernoch et al., 1991, Fig. 3 at −10 mV in this paper, and in many experiments not shown).

Recent studies (Hui, C. S., 1991) found a substantially greater temperature effect on the kinetics of Q_γ than Q_β; this is consistent with a mechanism of Q_γ as proposed here, in which the generation of Q_γ requires Ca release, a process that may have a greater Q_{10} than charge movement. It is also consistent with the generation of Q_γ at an independent set of voltage senors, working in parallel with the generators of Q_β.

Studies of Voltage Dependence

These include voltage dependence of activation (Huang, 1982; Hui, 1983*a*, *b*; Vergara and Caputo, 1983; Hui and Chandler, 1990) and inactivation (Adrian and Peres, 1979; Rakowski, Best, and James-Kracke, 1985).

In the present papers the amplitude of I_γ, obtained by tetracaine subtraction or

protocol 1, depends nonmonotonically on voltage, going through a maximum at about −40 mV. This feature is satisfactorily accounted for by the Ca-binding model. By contrast, in the published work $Q_\gamma(V)$ is seen to increase monotonically and very steeply, with the maximum of steepness near −50 or −40 mV (Hui, 1983*a*, *b*; Vergara and Caputo, 1983; Hui and Chandler, 1990).

The present model predicts an extra movement of charge. Even though according to the model most of the extra charge will return during the ON, it may be included in the computation of area under the asymmetric current, as discussed by Szűcs et al. (1991), especially when the inward phase of I_γ is slow. However, the present model also predicts that contribution will become small or nil at high voltages, contradicting the results of Hui (1983*a*) and Vergara and Caputo (1983) showing monotonic increase in $Q_\gamma(V)$.

One reason for the discrepancy may be that in those observations the voltage excursions did not go beyond −20 mV and this may have precluded the observation of a reduction in Q_γ beyond the maximum. An exception is the plot by Hui (1983*a*) of differences in charge due to dantrolene sodium. In this detailed experiment (which is interpreted by the author as resulting in suppression of 3.2 nC/μF of charge with a Boltzmann distribution) there is a local maximum at −30 mV, not inconsistent with our observations. Admittedly, this maximum could be due to noise. A local maximum is again found in the experiment of Fig. 6 of the same paper, in which fairly reproducible measurements of charge at many voltages near threshold reveal greater effect of dantrolene sodium at −40 and −45 mV (~4 nC/μF reduction), than at −25 and −30 mV (1.7 nC/μF).

Recent work of Hui and Chandler (1988, 1991) uses the slow kinetics of I_γ at depolarized potentials to isolate its OFF transient (using a stepped-OFF protocol). These OFFs have none of the anomalous characteristics seen in the present paper. They are monophasic and have a steep, sigmoidal voltage dependence, with characteristics suitable for an independent species of charge. It is therefore possible that our interventions and the method of Hui and Chandler (1988) separate two different components of total charge movement.

However, our model generates well-behaved I_γ currents with monotonic OFFs that increase steeply with voltage, provided that the time course of local $[Ca^{2+}]$ or the release fluxes used as starting points do not relax sharply after the peak. This is illustrated with a simulation in Fig. 17. The top record is a release flux (for a pulse to −40 mV, altered as described in the figure legend) that reaches about the same peak value as the largest record in Fig. 11 but has a less marked decay after the peak. This record was used in simulations entirely similar to the ones of fiber #612, with the same parameters (Table II).

The figure shows the triadic Ca^{2+} transient and the current I_γ that resulted. This I_γ is well behaved, the OFF charge is large and monophasic, and its voltage dependence (not illustrated) can be steep, as it is determined at low voltages by the voltage dependence of the release flux. It also has essential equality of charges at ON and OFF. Therefore, the model can generate this type of current and voltage distribution, consistent with an independent charged species. A radical departure will only occur at higher voltages, when the charge carried will become smaller with our simulations, rather than saturate.

Therefore, it is possible that both our interventions and the stepped-OFF protocol separate I_γ adequately, and that the underlying release time courses are different in our experiments and those of Hui and Chandler (1988, 1991). A more sustained level of release during the pulse also results in monophasic ONs, without inward phases (Fig. 17). In agreement with this interpretation, inward phases during the ON are not prominent in the records of Hui and Chandler (1990).

Other observations of voltage dependence use measurements of capacitance as a function of voltage (Adrian and Peres, 1979, Huang, 1982). In this type of measurement a decay in Q_γ vs. V is more difficult to detect than in Q vs. V plots. The variable prepulse required should also cause variable Ca^{2+} release and a variable degree of inactivation of release.

Studies of Localization in the Cell Membranes

A serious objection to a role of Q_β in E-C coupling was raised by studies of Huang and Peachey (1989; cf. also Adrian and Huang, 1984*b*), who measured capacitance

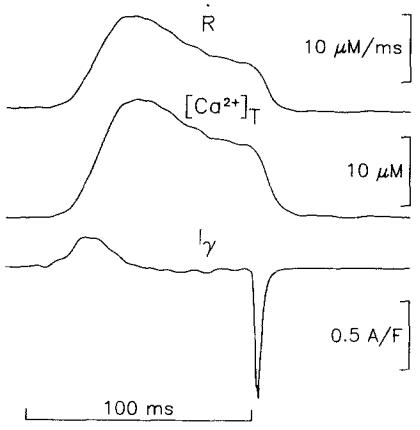

FIGURE 17. A simulated I_γ with simpler kinetics. $\dot{R}$, Release flux record with slow relaxation after the peak (obtained with a pulse to −40 mV from a h.p. of −90 mV in a fiber in 20 μM tetracaine, and scaled by a factor of 5.0). $[Ca^{2+}]_T(t)$, Triadic Ca^{2+} transient derived from $\dot{R}$, with the parameter values listed in Table II (fiber 612). I_γ, Charge movement current due to the Ca^{2+}-binding process, derived as described in the text with the parameter values in Table II (fiber 612).

changes upon detubulation, demonstrating that Q_γ moves in the t tubule membrane. In contrast, Q_β was found in equal proportion (that is, as an equal fraction of the accessible linear capacitance) in the T tubule and surface membranes.

This localization, however, is not inconsistent with the interpretation proposed here: If most E-C coupling takes place at the triadic junctions and Q_γ is a consequence of Ca release, then detubulation will preferentially reduce Q_γ. In contrast, Q_β is equated to all the tetracaine-resistant charge (Huang and Peachey, 1989) and is by definition a heterogeneous set. It could include currents from DHP-sensitive voltage sensors in the surface membrane not coupled to the SR, as well as gating currents from other channels. With this definition, it is not surprising that a fraction of Q_β resides in the surface membrane. For instance, and following Huang and Peachey's finding of proportional distribution, a 1:6 ratio of surface to T membrane area would result in a surface location for one-seventh of Q_β; this still leaves most of Q_β in the T system and is entirely consistent with a role of Q_β in E-C coupling.

Considering that 0.5 μM nifedipine reduces charge movement by ~22% at a holding potential of −100 mV, with almost no effect on Ca^{2+} release (Ríos and Brum, 1987), it is likely that some 20% of the total charge is unrelated to E-C coupling. If this charge was kinetically fast it would be counted as Q_β. Such a non-E-C coupling charge could be located anywhere; therefore, an equal distribution of Q_β in surface and tubules does not exclude a role of Q_β in E-C coupling.

In this regard, our simulation of I_β (Fig. 16) was not good at low voltages, missing a fast component. In other words, the steepness factor k used (11 mV) is too small to describe the broader distribution found in the experiment. There is in this particular experiment and fiber a fast component of small magnitude, moving at low voltage, which is not accounted for in the simulation. Problems inherent in the two Vaseline-gap technique (Chandler and Hui, 1990) complicate the interpretation of these small components.

Relationship between Q_γ and EC Coupling

Initial studies of the relationship between charge movement and Ca transients (Kovacs et al., 1979) were extended by Rakowski, Best, and James-Kracke (1985) and Melzer, Schneider, Simon, and Szűcs, (1986), who compared charge movement with Ca release flux, finding a much steeper dependence of release with voltage, particularly in the vicinity of the threshold voltage. Melzer et al. (1986) considered a sequential model in which the voltage sensor undergoes voltage-dependent subthreshold transitions before a final transition, also voltage-dependent, causes opening of the release channel (and moves a component of charge that is presumably Q_γ, even though their experimental records did not permit the kinetic identification of Q_γ). This model reproduced their results reasonably well but failed to generate the high steepness of release near threshold. In this regard, the proposal that Q_γ is an independent species directly linked to gating of Ca release is more satisfactory, as the steepness of Q_γ vs. V is greater than that of Q vs. V (cf. Hui and Chandler, 1988; Huang and Peachey, 1989). However, the steepness factors reported in the references above (5.5 and 3.9 mV) imply saturation of Q_γ at −20 mV (Huang and Peachey, 1989) or −40 mV (Hui and Chandler, 1988), while Ca release flux continues to increase at and beyond 0 mV (Brum et al., 1988*a*).

Other explorations of the relationship between Q_γ and E-C coupling have been carried out. Huang (1986) studied effects of twitch potentiators in intact fibers in hypertonic solutions, finding no change in the steady-state distribution of charge in the presence of 2.5 mM caffeine, a concentration that would have caused contracture had the fibers been able to respond mechanically. This is in contrast with the results in the third paper of this series, which showed a clear shift of the "hump" to more negative voltages at much lower caffeine concentrations. We cannot explain the discrepancy, but it should be noted that the paper of reference does not show the effects of caffeine on records of ΔI_{cm} or I_γ. Kinetic effects like the ones described by Szűcs et al. (1991) may have been overlooked when computing the charge distributions. If most of the charge returned during the ON (as in most records and simulations here), the change in $Q(V)$ would have been very small.

A similar discrepancy exists between the results in this series and the report of Csernoch et al. (1988), in which the effects of tetracaine on charge movements and

Ca transients were studied in cut fibers in a single Vaseline gap. 25 μM tetracaine reduced the Ca transient (by 40%) but not the distribution of total charge. This observation is again in contrast to our explanation of Q_γ (that significant changes in $[Ca^{2+}]_T$ should change Q_γ) and is also in conflict with the observations in three papers of this series, in which 20 or 25 μM tetracaine causes a substantial reduction in I_γ. Again, the discrepancy with Csernoch et al. (1988) is one of steady-state distribution of charge only; it can be reconciled if one considers the effects on the currents. Referring to Fig. 2 in Csernoch et al. (1988), record *B* of charge movement current, obtained in the presence of tetracaine, lacks a small delayed component present in reference record *A*. This effect, clear in the current records, does not change the area under the curve significantly. Therefore, the observations of Csernoch et al. (1988) are not inconsistent with the notion that I_γ is a consequence of release.

In closing, a summary of the main consequences of the present papers seems necessary. The delayed or "hump" component of charge movement current appears to be a consequence of Ca release. If, as the results seem to indicate, it involves additional voltage sensors from the same pool that generates I_β, it will cause opening of additional release channels. Thus, I_γ would be both consequence and cause of Ca release. I_β is likely to arise from heterogeneous sources, including voltage sensors of EC coupling, plus contributions from other voltage-sensitive molecules.

APPENDIX I

Linear Capacitive Currents in a Ca^{2+} Binding Process

When presenting these ideas we were asked (by Dr. F. Sigworth and Dr. J. Fernández) to evaluate how much linear capacitive charge would move upon binding of Ca^{2+} to one side of the membrane. We address this question here; the answer justifies neglecting linear currents in the simulations of I_γ.

Consider a simple situation: initially (Fig. 18 *A*) a membrane of dielectric permittivity $\epsilon\epsilon_0$ separates compartments e and i. The (bulk) potential difference V_{ie} is kept at zero by an external voltage clamp circuit. For simplicity, no fixed charges are present; thus, no surface potentials exist and the electric potential, $V(x)$, represented by the horizontal line, is the same everywhere.

At some instant, positive ions separate from solution i and bind to the surface of the membrane on the i side. As a consequence, charges move on both sides of the membrane. After a transient in which the voltage clamp circuit supplies some current to keep the bulk potential difference at 0 mV, a new steady potential $V(x)$ is established (Fig. 18 *B*), in which the local or microscopic transmembrane potential is positive. This is analogous to the model in this paper, except that here the membrane is initially uncharged (the distribution of V in our model can be easily found by superposition and is not important for the argument).

A standard procedure from electrostatics tells how much current circulates in the external circuit in the transition to the new equilibrium. Let the dotted line in Fig. 18 *B* represent a Gauss surface with two faces (of area A) parallel to the membrane, one within the membrane thickness and the other beyond the diffuse layer of unbalanced charge, sufficiently far from the membrane that V is constant. Applying to this surface the integral form of Gauss's law (e.g., Jackson, 1962, pp. 4, 5, and 616):

$$\epsilon\epsilon_0 \int_s E_n dA = q \tag{A1}$$

where E_n is the component of the electric field normal to the surface (in the outward direction) and q is the net charge within the surface. This field is zero everywhere on the surface except at the face within the membrane, where its value is termed E_m. Thus the integral in Eq. A1 is $-E_mA$. E_m in turn is the (microscopic) transmembrane voltage difference V_m divided by the membrane thickness l. Substituting in Eq. A1:

$$-\epsilon\epsilon_0 E_m A = -(\epsilon\epsilon_0 A/l)V_m = q \tag{A2}$$

The factor in parentheses is equal to the capacitance of the portion of membrane of area A. The charge q, which is the charge that moves in the external circuit, is equal to the membrane capacitance multiplied by the transmembrane potential. Thus, the same linear current moves per unit area whether the membrane is charged locally or through a bulk potential change.

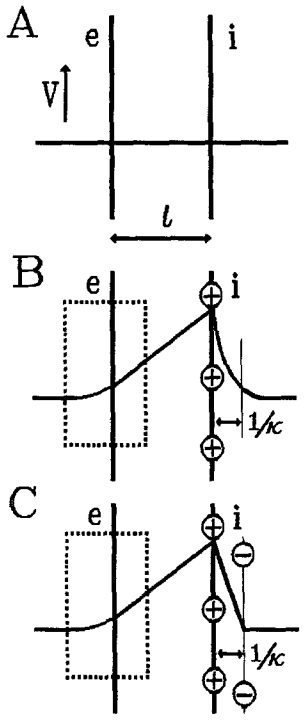

FIGURE 18. Capacitive charges induced by binding of ions. (*A*) An idealized situation: a membrane without charges separates two isopotential compartments. (*B*) Positive ions separate from solution i and bind to the i surface of the membrane. Counterions move toward the membrane on both sides. The result is an accumulation of negative charge (q) on side e, which results in a (capacitive) current from e to i measured in the external circuit. A Gauss surface is represented by dotted lines and is used to derive Eq. A2. (*C*) The distribution of counterions in i is modeled as a capacitor, with all ions at a distance equal to the Debye length $1/K$. The potential drop (V_s) across this capacitor is greater than the microscopic transmembrane potential (V_m). See Appendix I for details.

Unlike a bulk potential change, however, a local charging process might be restricted to a small area of the membrane. This would be the case, for instance, if the Ca^{2+} binding sites were on the voltage sensor protein. In this case only a fraction of the membrane capacitance would be affected by the change in potential, and the linear component in the current would be small.

It is simple to put an upper limit on this contribution. The excess charge on the e side (q) is negative. The excess charge on the opposite side is positive and of the same magnitude. This excess charge results from the (positive) Ca^{2+} ions bound and a diffuse layer of excess anions in solution. Thus, the linear capacitive charge that moves per unit area is less than the density of ions bound. The excess charge of counterions on the i side (q_c) can be estimated simply from a parallel plate capacitor model of the diffuse double layer illustrated in Fig. 18 *C* (McLaughlin, 1977) in which all the counterions are located at a distance from the membrane equal to the

Debye length ($1/K$). The difference in potential across this model capacitor is greater than V_m. Thus the charge q_c will be greater, in absolute value, than V_m multiplied by the equivalent capacitance of the diffuse layer

$$|q_c| > [\epsilon_r \epsilon_0 A/(1/K)]V_m \tag{A3}$$

where ϵ_r is the dielectric constant in the solution. The r.h.s. of Eq. A3 has the same form as Eq. A2, but is at least 10-fold greater, as the Debye length is $\sim 0.1\ l$ and $\epsilon_r > \epsilon$. Thus the anion charge q_c is much greater than q, which makes it approximately equal to the charge in the bound Ca^{2+}. This permits us to estimate an upper bound for q given the density of bound Ca^{2+}.

Assuming, for instance, 2,000 Ca^{2+} ions bound per square micrometer of T membrane (or ~ 4 per foot), the bound charge will be 6.4×10^{-8} C/cm^2. The charge q will be at least 10 times less, or $< 6.4 \times 10^{-9}$ C/cm^2. This amount will change the voltage in a 1-μF capacitor by 6.4 mV. In summary, the charge that moves in the external circuit when four Ca^{2+} bind per foot could change the voltage by at most 6.4 mV, and this is probably a gross overestimate.

APPENDIX II

Computer Simulations of Diffusion of Ca^{2+} in a Sarcomere

The thrust of these simulations is to obtain the approximate time course of $[Ca^{2+}]$ at a location near the sites of release. This is performed by means of a generalization of an earlier model of removal of Ca^{2+} introduced by Brum et al. (1988*a*), which will be called the "lumped" removal model to distinguish it from the present, distributed model.

The concentration of Ca^{2+} at any point in the sarcomere is the result of input and removal fluxes. The input flux for the whole sarcomere occurs at discrete points at the triads. Ca^{2+} spreads from there by diffusion and binds as it moves to structures that may be fixed (like sites on troponin or the SR pump) or slowly diffusing (parvalbumin, the Ca-sensitive dye).

In the present simulation the geometry of the sarcomere is one-dimensional (coordinate x) and symmetrical. The length of a half sarcomere is divided in $n + 1$ segments (that is, the half sarcomere is divided in $n + 1$ slices, represented by the index j, j = 0 to n). The first slice represents the triadic compartment and has thickness l. In a sarcomere of length L the other slices have thickness

$$(L - 2l)/(2n) \equiv \Delta x$$

The input of Ca^{2+} into the system occurs at $x = 0$ and has the time dependence of the Ca^{2+} release waveform $\dot{R}(t)$ measured experimentally. The purpose of the calculation is to obtain $[Ca^{2+}]\ (t, 0)$, the concentration of Ca^{2+} in the first compartment. As Ca^{2+} enters the jth compartment it can bind to parvalbumin, the dye ApIII, troponin, sites on the Ca^{2+} pump, and EGTA if present, according to the equations:

$$\mathrm{d[CaPar]}/\mathrm{d}t = k_{oncp}[Ca^{2+}][\mathrm{Par}] - k_{ofcp}[\mathrm{CaPar}] \tag{A4}$$

$$\mathrm{d[D_2Ca]}/\mathrm{d}t = k_{oncd}[Ca^{2+}][\mathrm{D}^2] - k_{ofcd}[\mathrm{D_2Ca}] \tag{A5}$$

$$\mathrm{d[CaTn]}/\mathrm{d}t = k_{onct}[Ca^{2+}][\mathrm{Tn}] - k_{ofct}[\mathrm{CaTn}] \tag{A6}$$

$$\mathrm{d[CaPp]}/\mathrm{d}t = k_{oncpp}[Ca^{2+}][\mathrm{Pp}] - k_{ofcpp}[\mathrm{CaPp}] \tag{A7}$$

$$\mathrm{d[CaEGTA]}/\mathrm{d}t = k_{once}[Ca^{2+}][\mathrm{EGTA}] - k_{ofce}[\mathrm{CaEGTA}] \tag{A8}$$

and is pumped away at a rate

$$\mathrm{d}[T]/\mathrm{d}t = M\{[\mathrm{CaPp}]/([\mathrm{Pp}] + [\mathrm{CaPp}])\}^2 \tag{A9}$$

while Mg^{2+} competes with Ca^{2+} for parvalbumin

$$d[MgPar]/dt = k_{onmp}[Mg^{2+}][Par] - k_{ofmp}[MgPar] \tag{A10}$$

Par, D, Tn, Pp, and EGTA represent parvalbumin, ApIII, troponin, pump sites, and EGTA in compartment j; CaPar, CaD_2, etc. are the bound forms of calcium, MgPar is the Mg^{2+}:parvalbumin complex, [T] is the rate of calcium transport by the pump per unit myoplasmic volume, and the k's are rate constants with self-explanatory subindices. There are no differences up to this point between this treatment of the removal processes within a slice and the lumped model of Brum et al. (1988*a*) in which the whole cell is considered a single compartment.

Additionally, the free Ca^{2+} can diffuse into the neighboring slices according to Fick's law, which was expressed in a difference equation for the flux between compartments. Let $[Ca^{2+}]$ (t, j) represent $[Ca^{2+}]$ at time t in slice j and let $d[Ca^{2+}]_{dif}/dt$ represent the rate of change of $[Ca^{2+}]$ in compartment j due to diffusional flux from j − 1 and j + 1 into j. This rate of change in concentration has different expressions for the first slice (0), the second (1), and a generic slice (j). Assume a diffusion coefficient D, unit section area, and let

$$\Delta x' \equiv (\Delta x + l)/2$$

Then, for the first slice:

$$\frac{d[Ca^{2+}]_{dif}(t, 0)}{dt} = D\left[\frac{[Ca^{2+}](t, 1) - [Ca^{2+}](t, 0)}{\Delta x'}\right]/l \tag{A11}$$

For the second slice:

$$\frac{d[Ca^{2+}]_{dif}(t, 1)}{dt} = D\left[\frac{[Ca^{2+}](t, 0) - [Ca^{2+}](t, 1)}{\Delta x'} + \frac{[Ca^{2+}](t, 2) - [Ca^{2+}](t, 1)}{\Delta x}\right]/\Delta x \tag{A12}$$

and for the generic slice:

$$\frac{d[Ca^{2+}]_{dif}(t, j)}{dt} = D\frac{[Ca^{2+}](t, j - 1) - [Ca^{2+}](t, j) + [Ca^{2+}](t, j + 1) - [Ca^{2+}](t, j)}{\Delta x^2} \tag{A13}$$

In the last compartment, j = n, a symmetry (reflecting) condition is added that insures no flux to or from the next half sarcomere

$$[Ca^{2+}](t, n) = [Ca^{2+}](t, n + 1) \tag{A14}$$

Finally, if $d[CaB](t, j)/dt$ represents the sum of all binding and removal rates (Eqs. A4 to A9), the equation describing the total rate of change of $[Ca^{2+}]$ can be written. For the first slice it is

$$\frac{d[Ca^{2+}](t, 0)}{dt} = -\frac{d[CaB](t, 0)}{dt} + \dot{R}(t) + \frac{d[Ca^{2+}]_{dif}(t, 0)}{dt} \tag{A15}$$

and for all others

$$\frac{d[Ca^{2+}](t, j)}{dt} = -\frac{d[CaB](t, j)}{dt} + \frac{d[Ca^{2+}]_{dif}(t, j)}{dt} \tag{A16}$$

The parameters (k's of removal and binding, M, concentrations of the various ligands) are obtained as described by Brum et al. (1988*a*) from fitting the lumped removal model predictions to the OFFs of the experimental Ca^{2+} transients. The sole parameter that is new in the distributed model is the diffusion coefficient of Ca^{2+}. This, following considerations of Kushmerick and Podolsky (1969) is taken to be 2.5 times smaller than the diffusion coefficient of Ca^{2+} in water, or 2.8×10^{-6} cm^2/s.

The system of Eqs. A3 to A16 was solved numerically by the unmodified Euler's method. The "Euler increment" of time (Δt) was routinely 5×10^{-6} s. Tests with values of the rate constants higher than the ones listed in Table II produced results that were consistent to better than 1% when using $\Delta t = 5 \times 10^{-6}$ s or 1×10^{-6} s. Increasing Δt beyond 10^{-5} s usually led to catastrophic overflow.

A total of 9 slices per half sarcomere gave essentially the same results in the triadic compartment as 17 slices. The width l of the first slice was set to 4 nm on the basis of volume considerations made by Csernoch et al. (1991). With this choice the volume ratio of triad to bulk is 500 in a stretched sarcomere (half length 2 μm) and ~300 in a slack sarcomere (1.3 μm). Even though we did not explore this variable systematically, we had the impression that a thickness of 20 nm resulted in very similar waveforms of $[Ca^{2+}]_T$. Finally, it made no qualitative difference whether parvalbumin and the dye were allowed to diffuse as well. In computations in which they diffused, a reflecting condition like Eq. A14 was introduced for each of the diffusing species.

One test of consistency for this simulation was suggested by one of our referees. Since the simulation results in time courses of all bound and free species in the model for all slices, it is possible to reconstruct the time course of total Ca:dye complex (proportional to the optical signal that the model predicts) and process it as one would an experimental signal to obtain a Ca^{2+} transient which we term $[Ca^{2+}]_s$. This is the Ca^{2+} transient that the model predicts for the particular $\dot{R}(t)$ used as input. In other words, if the fiber worked like the model and a flux of Ca^{2+} was dumped into it from the triads at a rate $\dot{R}(t)$, the dye would report a transient equal to $[Ca^{2+}]_s$.

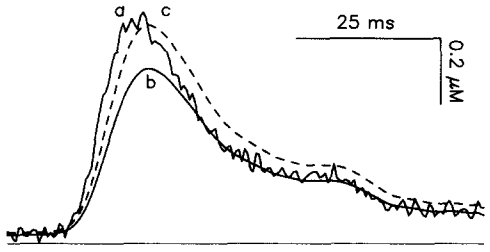

FIGURE 19. A test of consistency of the simulations. *a*, Measured Ca^{2+} transient during a pulse to −50 mV (same transient shown in Fig. 1). This transient was filtered and used to derive release flux, and the release flux was used as input of the simulation of diffusion (parameters in Table II). The simulation resulted in functions $[CaD_2](t, j)$ (j from 0 to 8). These functions were averaged over j, with weights corresponding to the thickness of the corresponding slices, and the resulting average was converted to $[Ca^{2+}](t)$ as in the usual determinations of Ca^{2+} transients. *b* is the derived transient, *c* is *b* scaled by 1.24.

This means that $[Ca^{2+}]_s$ should be close to the experimental $[Ca^{2+}]$ transient. If it is not, it means that the diffusion simulation, the method used to derive $\dot{R}(t)$, or both, are wrong. This rather crucial test is illustrated in Fig. 19. Record *a* is the Ca^{2+} transient measured during the pulse to −50 mV in fiber #612 (a record already shown in Figs. 1 and 2). *b* is the corresponding $[Ca^{2+}]_s$ obtained in the simulation of diffusion that led to the records in Fig. 12. *c* is *b* scaled by 1.24. The agreement is reasonable.

Fibers #650 and #651 included in Fig. 5 were studied by Dr. Adom González and Dr. Ivan Stavrovsky at Rush University. We owe them gratitude for allowing the inclusion of these data in this paper. We are grateful to Drs. Fredric Cohen, R. S. Eisenberg, and Jianjie Ma for many suggestions, to Drs. C. S. Hui and W. K. Chandler for communicating several unpublished results, and to Ms. Lucille Vaughn for typing the manuscript.

This work was funded by grants from the NIH (R01-AR-32808) and MDA.

Original version received 28 November 1989 and accepted version received 12 September 1990.

REFERENCES

Adrian, R. H., and W. Almers. 1976. The voltage dependence of membrane capacity. *Journal of Physiology.* 254:317–338.

Adrian, R. H., and C. L. H. Huang. 1984*a*. Charge movements near the mechanical threshold in skeletal muscle of *Rana temporaria*. *Journal of Physiology.* 349:483–500.

Adrian, R. H., and C. L. H. Huang. 1984*b*. Experimental analysis of the relationship between charge movement components in skeletal muscle of *Rana temporaria*. *Journal of Physiology.* 353:419–434.

Adrian, R. H., and A. Peres. 1977. A gating signal for the potassium channel? *Nature.* 267:800–804.

Adrian, R. H., and A. Peres. 1979. Charge movement and membrane capacity in frog muscle. *Journal of Physiology.* 289:83–97.

Almers, W., R. H. Adrian, and S. R. Levinson. 1975. Some dielectric properties of muscle membrane and their possible importance for excitation-contraction coupling. *Annals of the New York Academy of Science.* 264:278–292.

Baylor, S. M., M. E. Quinta-Ferreira, and C. S. Hui. 1985. Isotropic components of Antipyrylazo III signals from frog skeletal muscle fibers. *In* Calcium in Biological Systems. R. P. Rubin, G. Weiss, and J. W. Putney, Jr., editors. Plenum Publishing Corp., New York. 339–349.

Brum, G., R. Fitts, G. Pizarro, and Ríos. 1988*a*. Voltage sensors of the frog skeletal muscle membrane require calcium to function in excitation-contraction coupling. *Journal of Physiology.* 398:475–505.

Brum, G., and E. Ríos. 1987. Intramembrane charge movement in frog skeletal muscle fibres: properties of charge 2. *Journal of Physiology.* 387:489–517.

Brum, G., E. Rios, and E. Stefani (with an appendix by G. Brum, E. Ríos, and M. F. Schneider). 1988*b*. Effects of extracellular calcium on the calcium movements of excitation-contraction coupling in frog skeletal muscle fibres. *Journal of Physiology.* 398:441–473.

Chandler, W. K., and C. S. Hui. 1990. Membrane capacitance in frog cut twitch fibers mounted in a double Vaseline–gap chamber. *Journal of General Physiology.* 96:225–256.

Csernoch, L., C. L. H. Huang, L. Kovacs, and G. Szűcs. 1987. Charge movement components and calcium transients in isolated frog skeletal muscle fibers. *Journal of Physiology.* 382:165P.

Csernoch, L., C. L.-H. Huang, G. Szűcs, and L. Kovacs. 1988. Differential effects of tetracaine on charge movements and Ca^{2+} signals in frog skeletal muscle. *Journal of General Physiology.* 92:601–612.

Csernoch, L., G. Pizarro, I. Uribe, M. Rodríguez, and E. Ríos. 1991. Interfering with calcium release suppresses I_γ, the "hump" component of intramembranous charge movement in skeletal muscle. *Journal of General Physiology.* 97:845–884.

Duane, S., and C. L.-H. Huang. 1982. A quantitative description of the voltage-dependent capacitance in frog skeletal muscle in terms of equilibrium statistical mechanics. *Proceedings of the Royal Society of London, Section B.* 215:75–94.

García, J., G. Pizarro, E. Ríos, and E. Stefani. 1991. Effect of the calcium buffer EGTA on the "hump" component of charge movement in skeletal muscle. *Journal of General Physiology.* 97:885–896.

Heiny, J., D. Jong, S. H. Bryant, D. Conte Camerino, and V. Tortorella. 1990. Enantiomeric effects on excitation-contraction coupling in frog skeletal muscle by a chiral phenoxy carboxylic acid. *Biophysical Journal.* 57:147–152.

Hollingworth, S., and M. W. Marshall. 1981. A comparative study of charge movement in rat and frog skeletal muscle fibres. *Journal of Physiology.* 321:583–602.

Hollingworth, S., M. W. Marshall, and E. Robson. 1987. Absence of tetracaine-sensitive charge components in rat isolated skeletal muscle. *Journal of Physiology.* 391:89P.

Hollingworth, S., M. W. Marshall, and E. Robson. 1990. The effects of tetracaine on charge movement in fast twitch rat skeletal muscle fibres. *Journal of Physiology.* 421:633–644.

Huang, C. L. H. 1982. Pharmacological separation of charge movement components in frog skeletal muscle. *Journal of Physiology.* 324:375–387.

Huang, C. L. H. 1984. Analysis of 'off' tails of intramembrane charge movements in skeletal muscle of *Rana temporaria*. *Journal of Physiology*. 356:376–390.

Huang, C. L. H. 1986. The differential effects of twitch potentiators on charge movements in frog skeletal muscle. *Journal of Physiology*. 380:17–33.

Huang, C. L. H. 1987. 'Off' tails of intramembrane charge movements in frog skeletal muscle in perchlorate containing solutions. *Journal of Physiology*. 384:491–510.

Huang, C. L. H. 1989. Intramembrane charge movements in skeletal muscle. *Physiological Reviews*. 68:1197–1247.

Huang, C. L. H., and L. D. Peachey. 1989. The anatomical localization of charge movement components in frog skeletal muscle. *Journal of General Physiology*. 93:565–584.

Hui, C. S. 1983*a*. Pharmacological studies of charge movement in frog skeletal muscle. *Journal of Physiology*. 337:509–529.

Hui, C. S., 1983*b*. Differential properties of two charge components in frog skeletal muscle. *Journal of Physiology*. 337:531–552.

Hui, C. S. 1991. Comparison of charge movement components in intact and cut twitch fibers of the frog. Effects of stretch and temperature. *Journal of General Physiology*. In press.

Hui, C. S., and W. K. Chandler. 1988. Currents associated with intramembranous charge movement in frog cut twitch fibers. *Biophysical Journal*. 53:646*a*. (Abstr.)

Hui, C. S., and W. K. Chandler. 1990. Intramembranous charge movement in frog cut twitch fibers mounted in a double Vaseline-gap chamber. *Journal of General Physiology*. 96:257–298.

Hui, C. S., and W. K. Chandler. 1991. Q_β and Q_γ components of intramembranous charge movement in frog cut twitch fibers. *Journal of General Physiology*. In press.

Jackson, J. D. 1962. Classical Electrodynamics. John Wiley & Sons, Inc., New York, London. 4, 5, 616.

Kovacs, L., E. Ríos, and M. F. Schneider. 1979. Calcium transients and intramembrane charge movement in skeletal muscle fibers. *Nature*. 279:391–396.

Kovacs, L., E. Ríos, and M. F. Schneider. 1983. Measurement and modification of free calcium transients in frog skeletal muscle fibres by a metallochromic indicator dye. *Journal of Physiology*. 343:161–196.

Kushmerick, M. J., and R. J. Podolsky. 1969. Ionic mobility in muscle cells. *Science*. 166:1297–1298.

Lamb, G. D. 1986*a*. Asymmetric charge movement in contracting muscle fibres in the rabbit. *Journal of Physiology*. 376:63–83.

Lamb, G. 1986*b*. Components of charge movement in rabbit skeletal muscle: the effects of tetracaine and nifedipine. *Journal of Physiology*.

McLaughlin, S. G. A. 1977. Electrostatic potentials at membrane-solution interfaces. *Current Topics in Membrane Transport*. 9:71–144.

Melzer, W., E. Ríos, and M. F. Schneider. 1984. Time course of calcium release and removal in skeletal muscle fibers. *Biophysical Journal*. 45:637–641.

Melzer, W., E. Ríos, and M. F. Schneider. 1987. A general procedure for determining calcium release in skeletal muscle fibers. *Biophysical Journal*. 51:849–864.

Melzer, W., M. F. Schneider, B. Simon, and G. Szűcs. 1986. Intramembrane charge movement and Ca release in frog skeletal muscle. *Journal of Physiology*. 373:481–511.

Pizarro, G., M. Rodríguez, L. Csernoch, and E. Ríos. 1990. Positive feedback in skeletal muscle E-C coupling. *Biophysical Journal*. 57:401*a*. (Abstr.)

Rakowski, R. F., P. M. Best, and M. R. James-Kracke. 1985. Voltage dependence of membrane charge movement and calcium release in frog skeletal muscle fibres. *Journal of Muscle Research and Cell Motility*. 6:403–433.

Ríos, E., G. Brum, G. Pizarro, and M. Rodríguez. 1990. Effects of calcium buffers on calcium transients in skeletal muscle fibers. *Biophysical Journal*. 57:341*a*. (Abstr.)

Simon, B. J., and K. G. Beam. 1985. The influence of transverse tubular delays on the kinetics of charge movement in mammalian skeletal muscle. *Journal of General Physiology.* 85:21–42.

Smith, P. D., G. L. Liesegang, R. L. Berger, G. Czerlinski, and R. L. Podolsky. 1984. A stopped-flow investigation of calcium ion binding by ethylene glycol bis(β-aminoethyl ether)-N,N′-tetraacetic acid. *Analytical Biochemistry.* 143:188–195.

Szűcs, G., L. Csernoch, J. Magyar, and L. Kovács. 1991. Contraction threshold and the "hump" component of charge movement in frog skeletal muscle. *Journal of General Physiology.* 97:897–911.

Vergara, J., and C. Caputo. 1983. Effects of tetracaine on charge movements and calcium signals in frog skeletal muscle fibers. *Proceedings of the National Academy of Sciences, USA.* 80:1477–1481.